ALBUMIN-DERIVED NANOPARTICLES: A FLEXIBLE BIOINTERFACE FOR ENHANCED ADHESION, SPATIAL GUIDANCE AND GROWTH FACTOR STIMULATION OF HUMAN MESENCHYMAL STEM CELLS

by

JING XU

A thesis submitted to the

Graduate School-New Brunswick

Rutgers, The State University of New Jersey

and

The Graduate School of Biomedical Sciences

University of Medicine and Dentistry of New Jersey

In partial fulfillment of the requirements

For the degree of

Master of Science

Graduate Program in Cell and Developmental Biology

Written under the direction of

Prabhas V. Moghe

And approved by

_____

_____

_____

New Brunswick, New Jersey

May 2010

ABSTRACT OF THE THESIS

ALBUMIN-DERIVED NANOPARTICLES: A FLEXIBLE BIOINTERFACE FOR ENHANCED ADHESION, SPATIAL GUIDANCE AND GROWTH FACTOR STIMULATION OF HUMAN MESENCHYMAL STEM CELLS

By JING XU

Thesis Director:

Prabhas V. Moghe

Mesenchymal stem cells (MSCs) are multipotent stem cells that can differentiate into a variety of cell types and have been widely investigated as a possible alternative treatment strategy for wound healing. A major challenge to the direct application of MSCs in severe wounds is the limited engraftment of these cells at the wound sites (<1%) and a lack of spatial control of MSC adhesion and activation, which could be potentially enhanced through engineered nanoscale multifunctional substrates. The use of human albumin-derived nanoparticles (ANPs) as a foundational nanoscale substrate to display RGD-containing fibronectin $FIII_{9-10}$ fragment (Abbreviated: Fnf) has been previously reported in the Moghe laboratory. When presented in 2-D cell cultures on ANPs, this ligand has been proven to promote cell motility and extracellular matrix assembly. Here we showed Fnf-ANPs promoted human MSCs (hMSCs) adhesion as well as integrin clustering in cell protrusions and were able to spatially direct the adhesion and growth of hMSC on 2-D polymer substrates. Furthermore, hMSC morphology and its organization of focal adhesion were

sensitively modulated by nanoscale size of ANPs. The adhesion of hMSC was cooperatively promoted in the presence of Fnf-ANPs and growth factor, bFGF. In order to promote similar synergies between the biofunctionalized ANPs and growth factors, we engineered albumin nanoparticles with P14 peptide, a fibronectin-derived growth factor sequestering peptide proven to bind to a variety of growth factors. Thus, we demonstrate that albumin-derived nanoparticles can be used as a flexible system for nanoscale presentation of adhesion and growth factors, the combination of which could potentially control hMSC phenotype and functions.

DEDICATION

To my parents and my husband Eddie

ACKNOWLEDGEMENT

I am sincerely thankful to my thesis advisor, Dr. Prabhas Moghe, whose encouragement, guidance and support from the initial to the final enabled me to develop an independent research project and obtain solid research training. I also have deepest gratitude for the members of my supervisory committee, Dr. Li Cai and Dr. Ramsey Foty, without whose knowledge, assistance and encouragement this study would not have been successful. I especially acknowledge them for spending their precious time to read this thesis and gave their critical comments about it. I also want to thank Dr. Debabrata Banerjee as my IGERT co-advisor. I am much indebted for his valuable advice in science discussion and supervision in MSC biology and wound healing mechanisms.

I would also like to thank Dr. Henry Hsia, Dr. Robert Harris and Dr. David Reimer for their comments and advice on wound-healing animal models. Furthermore, I would like to thank all Moghe group members for their invaluable support and care for the last three years. Dr. Mará Pá Rossi and Dr. Craig Griffith gave me tremendous help and guidance in my research. I would also like to thank all other team members, Dominik Naczynski, Jocie Cherry, Er Liu, Aaron Carlson, Nicole Plourde, Tamar Andelman, Joe Kim, Sebastian Vega, Kubra Kamisoglu, Daniel Lewis, who are always there for me. I also wish to express my love and gratitude to my beloved families for their understanding and endless love through the duration of my studies. Lastly, I'd like to thank all of those who supported me in any respect during the completion of the project.

TABLE OF CONTENTS

LIST OF TABLES

LIST OF ILLUSTRATIONS

CHAPTER 1: INTRODUCTION

1.1 Background and Significance

1.1.1 Clinical Impetus

Chronic wounds are wounds that do not heal within three months [2]. They fail to progress through the normal healing stages and therefore enter a prolonged period of chronic inflammation. The prevalence of chronic wounds is estimated to be around 4 million in the United States with the overall incidence of chronic wounds is around 0.78% of the population and the majority of the patients (~85%) are older than 65 [3]. Chronic wounds result in enormous health care cost estimated at more than $3 billion per year. Around 70% of chronic wounds are caused by ischemia, secondary to diabetes, venous stasis, and pressure [4] and almost all chronic wounds have similar impaired healing progressions as well as similar inflammatory profiles. Overactive inflammation, poor local circulation, and/or the presence of the necrotic tissue are main pathological characterizations [5]. Consequently, the healing process is inhibited, resulting in incomplete anatomical repair and physiological function.

Chronic wounds have prolonged inflammatory phase. Over-activated inflammatory cells such as the phagocytes, neutrophils, and macrophages secrete elevated levels of pro-inflammatory cytokines such as tumor necrosis factor-α (TNF-α) and the interleukins (IL): IL-1, IL-6, and IL-8 [6]. Moreover, high levels of proteases may also be present in chronic wounds. Therefore, growth factors and cell surface receptors can be proteolytically degraded in the chronic wound environment. Using dextranomer beads, Cooper and colleagues found

that levels of several growth factors were lower or even undetectable in many pressure ulcers [7]. Trengove et al found chronic wounds contain much higher level of matrix metalloproteinases (MMP), which can degrade growth factors such as epidermal growth factor (EGF) much faster than that from acute wounds [8]. In contrast, immunostaining indicated that expression of both TGF-β and its receptor were significantly increased in healing versus nonhealing leg ulcers [9].

There are several therapeutic modalities available for the treatment of chronic wounds. Since excessive inflammation is the ultimate cause of the poor healing found in chronic wounds, most treatments are aimed at reducing inflammation. Surgical debridement and wound care methods decrease the necrotic tissue and protease burden, thus providing a virtual resetting of the wound back into the acute healing phase. Another method for altering the inflammatory cascade involves using exogenous cytokines and growth factors. For example, platelet-derived growth factor–BB (PDGF-BB) is approved for use in the treatment of diabetic neuropathic ulcers, however, it has been of limited clinical value because 1) many chronic wounds do not respond; 2) it has to be used with caution in patients with known malignancy because there was a 5-fold increased risk of cancer mortality in the group exposed to 3 or more tubes of a commercialized human PDGF product—REGRANEX Gel (refer to http://www.regranex.com/). Even with recent advances in bioengineered artificial skin equivalent, up to 50% chronic wounds that have stayed unhealed for more than a year remain resistant to treatment [10]. With large chronic ulcers, autologous split-thickness or punch grafting can be successful with healing rates of up to 75% [11]. However, for patients with

chronic wounds, autologous skin graft is not an ideal choice as it introduces another wound that might not heal quickly. Cellular therapy is an emerging therapeutic strategy for cutaneous wounds. Application of cultured human skin derived cells (keratinocytes and fibroblasts), alone or combined with extracellular matrix (ECM) scaffolds to generate an ex vivo engineered skin equivalent, have shown some promise in decreasing the healing time of chronic wounds. For example, bi-layered skin construct (Apligraf®) was found to be effective in healing chronic ulcers faster. However, it is very expensive (given the annual medical cost of managing patients with hard-to-heal venous leg ulcers to be $20,041 for those treated with Apligraf® [12]) and cannot be used on the patients who are allergic to bovine collagen. Additionally, these composites have a short shelf-life. Due to these concerns, the potential of stem cell based cellular therapy to correct impaired healing holds great promise. So far, considerable focus has been placed on bone marrow–derived human mesenchymal stem cells (hMSCs), and this thesis work seeks to investigate the role of nanoscale biofunctionalized substrates to prime hMSCs for early management of chronic wounds.

1.1.2 Human Mesenchymal Stem Cells and Tissue Engineering

Human MSCs possess several advantages as candidates for cell-based therapy for accelerating wound healing. First, these cells can be induced to differentiate along specific lineages (stromal, adipogenic, osteogenic, chondrogenic) by growth in defined media [13]. These different lineages will deposit their own specific ECM thus providing several distinct microenvironments for cells at wound bed [14]. Secondly, MSCs have been previously

shown to mediate differentiation of other cell types [15]. While the exact mechanism is not known, it has been suggested that MSC differentiation and secretion of various cytokines contribute to this effect. Finally, MSCs are hypoimmunogenic and therefore are suitable for allogeneic transplantation and inflammation suppression [16]. MSCs express the surface ligand CD200, which turns off the adaptive immune response [17-19].

Several animal studies have already shown that application of MSCs can promote healing of chronic wounds. For example, application of allogeneic MSCs significantly accelerated wound closure in splinted excisional wound models on both normal and diabetic mice compared with using allogeneic neonatal dermal fibroblasts [20]. MSCs accelerated healing in part through their differentiation into wound myofibroblasts and their secretion of several different growth factors such as vascular endothelial growth factor (VEGF), basic fibroblast growth factor (bFGF) and other growth factors [21, 22]. MSCs also have been used in several clinical trials to affect tissue repair. For example, allogeneic bone marrow-derived mesenchymal stem cells were applied systematically in human patients afflicted with osteogenesis imperfecta, a genetic defect in bone and other tissues caused by mutations in the genes for type 1 collagen. Children who received therapy showed measurable improvements in growth velocity, bone mineral density, and ambulation despite the fact that the levels of engrafted donor MSCs in bone, skin, and other tissues were less than 1% [23]. Therefore, direct engraftment of allogeneic MSCs to wound bed using an optimized biocompatible delivery approach may be a particularly effective approach to augment therapeutic effect.

1.1.3 Nanoscale Bio-adhesive Ligand Presentation and Wound Healing

Cell-adhesive ECM-derived peptides or fragments, such as RGD-containing sequences, specifically bind to cell surface receptors and trigger the recruitment of downstream intracellular anchor proteins to the adhesion site, ultimately inducing the assembly of focal adhesions and the associated cytoskeleton molecules [24]. This process has been proven to be critical in cell adhesion, survival, migration as well as differentiation [25]. Maheshwari et al assessed the concentration dependence of RGD integrin interactions by varying the average surface density of the integrin ligands or by nanoscale clustering of YGRGD peptides [26]. These researchers reported that the clustering of ligand significantly reduced the average ligand density required to support cell migration while nonclustered integrin ligands elicited cell attachment but neither full spreading nor enhanced motility. They also showed variation in YGRGD presentation also affects the organization of actin filaments within the cell, with a greater number of cells exhibiting stress fibers at higher cluster sizes of YGRGD. By varying the spacing between the RGD-biofunctionalized gold dots, Cavalcanti-Adam et al modulated the clustering of the associated integrins and showed that the formation of stable focal adhesions and persistent spreading is sensitive to RGD density, indicating that RGD density plays an essential role for the establishment of mature and stable integrin adhesions, which, in turn, induce efficient cell spreading and formation of focal adhesions [27].

The ANP system was utilized for the presentation of the FNIII9-10 domain of fibronectin, a RGD-containing peptide which is fused with an N-terminal glutathione-S-transferase (GST) [28]. Albumin nanoparticles (ANPs) are fabricated from human albumin using previously

developed techniques based on pH and temperature changes to induce self-assembly of the albumin chains through intermolecular disulfide bonding [29] (Figure 1-1). The process

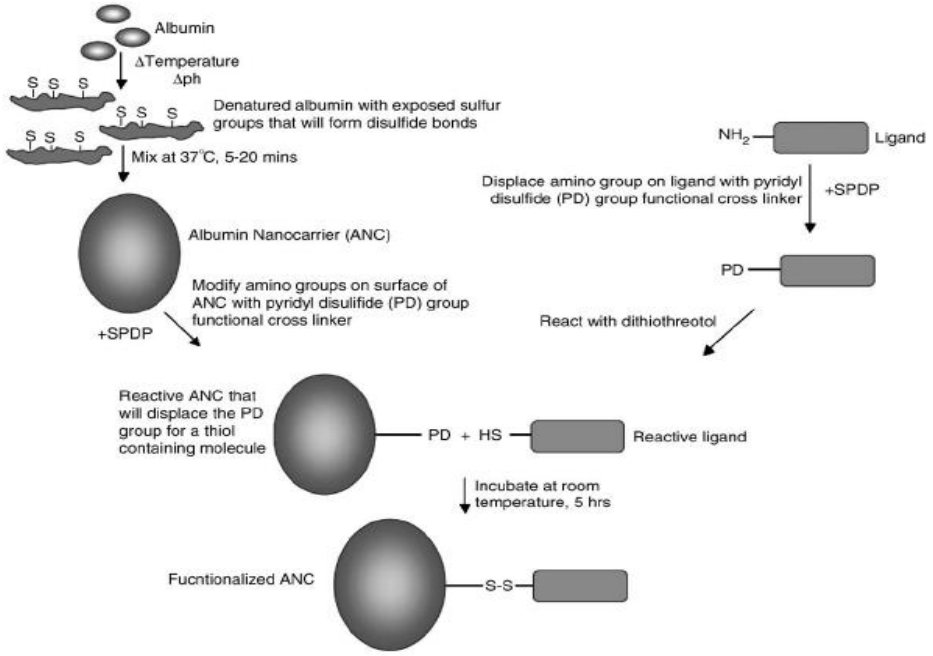

Figure 1-1. Schematic of the fabrication steps of Fnf-ANPs.

yields ANPs of controllable sizes ranging from 30-160nm and the size is proportional to the stirring time. Through collaborative studies between the Moghe lab (Rutgers University) and the Schwarzbauer lab (Princeton University), we have shown that ANPs can be functionalized with a fibronectin fragment (Fnf). The functionalized nanoparticles are abbreviated as Fnf-ANPs (Albumin Nanoparticles conjugated with Fibronectin Fragments) here. These functionalized ANPs were used to manipulate the behavior of cells such as primary human keratinocytes and fibroblasts [30]. Fnf is composed of a GST tag and a fibronectin fragment $FNIII_{9\text{-}10}$. The III9-10 domains include the 10th type III domain of fibronectin, which contains the RGD tri-peptide adhesion motif essential for integrin binding and stimulating downstream signaling pathways, as well as the neighboring 9th type III domain, which synergistically enhances integrin binding and signaling.

When presented as adhesive substrate for 2-D cell cultures on albumin-derived nanocarriers, this ligand can promote cell adhesion, motility and extracellular matrix assembly [29, 30]

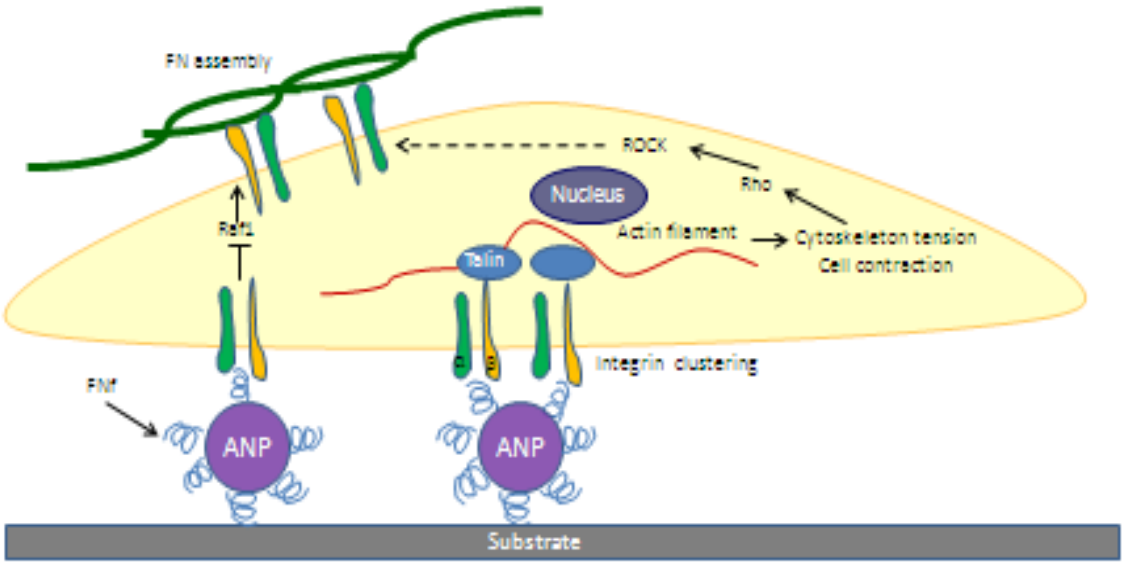

Figure 1-2. The binding of Fnf-ANPs and integrins enhances cell tension and subsequent FN assembly. matrix assembly was found to be correlated to nanoparticle size—fibronectin matrix assembly was greatest at the highest ligand density on larger-sized nanocarriers, but was undetectable at the same ligand density on smaller-sized carriers [1].

(Figure 1-2). Further, matrix assembly was found to be correlated to nanoparticle size—fibronectin matrix assembly was greatest at the highest ligand density on larger-sized nanocarriers, but was undetectable at the same ligand density on smaller-sized carriers [1]. The possible explanation could be that the increased inertia of larger-sized nanocarriers displaying adhesion ligands may generate more tension in the cytoskeleton, which, in turn, promotes morphological and phenotypic changes ultimately resulting in up-regulation of

downstream matrix assembly. Thus, the size of the nanoparticle and the density of ligand on that nanoparticle combine to dictate the early kinetics of fibroblast matrix assembly. The effects of Fnf-ANPs in the adhesion, spreading and migration of stem cells in general, and adult mesenchymal stem cells in particular, still remain to be characterized.

1.2 SUMMARY

The long term goal of this study is to investigate a combined biological and engineering approach to apply mesenchymal stem cells for treating chronic wounds. Chronic wounds are defined as wounds resistant to healing within three months. Since most chronic wounds occur in patients 65 years and older, autologous skin graft is not an ideal reconstructive choice because it introduces another wound that might not heal shortly. Even with recent advances in recombinant growth factors and bioengineered skin, up to almost 50% of chronic wounds remain resistant to treatment. MSCs are multipotent stem cells that can differentiate into a variety of cell types and have been recently investigated as a possible alternative treatment strategy for chronic wounds. Bone marrow derived MSCs (BM-MSCs) are immunosupressive and have been shown to mediate skin regeneration after transplantation in animals. RGD-containing $FNIII_{9-10}$ conjugated albumin nanoparticles have been shown by our lab to have significant effects in enhancing skin cell functions including migration, contractility and matrix assembly, in this work, we investigated the nanoscale presentation of RGD-containing peptide in the adhesion and migration of hMSCs and the possibility of developing a micropatterning technique to incorporate the biofunctionalized nanoparticles for cell adhesion guidance. Furthermore, a novel growth factor peptide was conjugated on the

same nanoparticle system as a means to selectively retain certain types of growth factors and provide specific soluble cues for stem cell differentiation.

CHAPTER 2: EFFECTS OF BIOFUNCTIONALIZED ALBUMIN NANOPARTICLES ON HUMAN MESENCHYMAL STEM CELL ADHESION, SPREADING AND MIGRATION

2.1 Abstract

The $FNIII_{9-10}$ domain of fibronectin contains the RGD motif necessary for cell-adhesive function and can be recognized by several integrin types. The clustering of integrin β1 has been previously implicated in the regulation of MSC adhesion, migration, and transmigration. Thus, the $FNIII_{9-10}$ fragment (abbreviated as Fnf) was conjugated to albumin nanoparticles (ANPs), and substrates based on the Fnf-ANPs were investigated for their effects on human mesenchymal stem cell adhesion and motility behaviors. We found that Fnf-ANPs play a role in regulating and possibly promoting MSC adhesion and migration in the presence of optimal growth factor/soluble stimulation. Different sizes of passively adsorbed Fnf-ANPs induced different cell morphologies and distribution of focal adhesion plaques, dendritic and unpolarized on small sized particles with less vinculin expression while fully polarized and more spread out on large sized particles with strong and fibrillar vinculin expression through the cell body. Taken together, it suggests a potential application of Fnf-ANPs in enhancing hMSC adhesion, migration in stem cell-based cellular therapy for chronic wounds.

2.2 Background and Rationale

The incorporation of bioactive peptides in as cellular support may enhance growth and other cell functions of MSC in vitro. Salinas et al found that the incorporation of tethered RGD peptide motifs enhanced hMSC survival when the cells were encapsulated in PEG hydrogel.

Moreover, staining of integrin $\alpha_v\beta_3$ and focal adhesion proteins were found to correlate to the trends in hMSC survival for covalently-bound RGD motifs [31]. In addition, covalently bound RGD motifs were shown to not only promote survival of hMSCs encapsulated in PEG gels but also to induce early stages of chondrogenesis [32]. Similarly, Alvarez-Barreto et al showed that the presence of RGDC on the surface of PLLA 2-D disks and 3-D scaffolds increased cell surface area and the number of adherent mesenchymal stem cells [33].

In chronic wounds, the balance between formation and degradation of ECM proteins is disrupted by high levels of local matrix metalloproteinases (MMPs). For instance, fibronectin in diabetic ulcer wound fluid was found partially degraded [34]. Moreover, the diabetic patients had a significantly lower plasma fibronectin level than the controls of the same age-groups [35]. Not only plasma fibronectin, tissue fibronectin was also found to be absent from the ulcer tissue biopsies [36]. This makes tissue regeneration by implanting biomaterial more challenging in chronic wounds than in other diseases. The following explains the reason. Generally, the first event of in vivo biomaterial implanting is the binding of serum proteins, vitamins and other molecules to the biomaterial, which enables subsequent cell adhesion and spreading. If the local cell-adhesive proteins such as fibronectin and collagen are insufficient and/or deficient, the surface modification from those adsorptions on the implant is not bio-adhesive enough to recruit host cells for tissue regeneration. Therefore, it is desirable to modify the surface of inert polymers to create biomimetic composites which are able to enhance biocompatibility and bioactivity. The aforementioned Fnf-ANPs will be used as a model biointerface on the poly(DTE carbonate) scaffolds for this purpose.

Moreover, it has been shown that integrin β_1 clustering plays a key role in MSC migration [37, 38]. Ip et al. used an in vivo model of acute myocardial infarction to define the contribution of selected candidate molecules by evaluating the blocking effect of specific monoclonal antibodies on allogeneic MSC transplantation into mouse heart. A significant reduction in the total number of MSC in the infarcted myocardium was observed after integrin β_1 blockade, indicating that integrin beta1 is important for MSC migration and engraftment in the infarcted myocardium [38]. By using a co-cultivation model of MSC and endothelial cells, Steingen et al proved that beta1 integrin was one of the key players involved in transmigration and invasion of MSCs [37]. RGD-containing Fnf will be used to functionalize the ANPs. We studied the effects of Fnf-ANPs in regulating and possibly promoting MSC adhesion and spreading.

2.3 Materials and Methods

2.3.1 ANP Synthesis and Functionalization

ANPs were synthesized and functionalized based on an established method [39]. Briefly, 30% (w/v) human serum albumin (Sigma, St. Louis, MO) was diluted to 1% with phosphate-buffered saline (PBS) and filtered through a 0.22 μm filter (Fisher Scientific, Pittsburgh, PA) to remove albumin aggregates. Next, the pH of the albumin solution was raised to 10.65 with 0.1 N NaOH, heated to 78 ℃ and maintained within the range of 78-82 ℃ for 10min. After cooling to room temperature (RT) in an ice bucket, the solution was maintained at RT for 10min. The pH was then lowered to 6.0 with 0.1 N HCl. The albumin solution was heated to

37℃ on a hot plate and stirred at intermediate rate to allow the self-assembly of albumin molecules through intermolecular disulfide bond formation. Nanoparticle size is the function of stirring time. Generally, 5ml of albumin sample was collected at 5, 10, 15 and 20min and further aggregation was stopped by reacting with 0.1% (w/v) iodoacetamide (Sigma, St. Louis, MO) as an aggregation stablizer for 1h at RT. Monomeric albumin (MW=66 kDa) was removed by dialysis (molecular weight cut off: 100 kDa) against PBS for three times. After sample collection from dialysis, albumin aggregates larger than 220 nm were removed from nanocarrier preparations by sterilization through a 0.22 μm filter. For functionalization, the Fnf and ANPs are reacted with N-Succinimidyl-3-(2-PyridylDithio)-Propionate (SPDP), a heterobifunctional cross-linking agent that reacts with free amine groups to form an amide linkage. The Fnf is further reacted with dithiothreitol (DTT), a reducing agent that generates free sulfhydryl group (-SH) on the Fnf by displacing the 2-pyridyldithiol (PD) group of the SPDP. The SPDP-ANPs and SH-Fnf are incubated together to allow disulfide bonding to form between both molecules. Excess Fnf not consumed in the conjugation reaction was removed from the conjugation products by dialysis (molecular weight cut off: 100 kDa) against PBS.

2.3.2 Nanoparticle Sizing

DLS was used to characterize the size and polydispersity of the ANPs [39]. Unfunctionalized nanoparticles were diluted 1:5 to 1:10 and 1ml of the diluted sample was added to the disposable polystyrene cuvettes (Malvern DTS0012). Then the cuvette was inserted into Dilute Dynamic light scattering (DLS) apparatus (Malvern Zetasizer) for sizing. Automatic

measurement setting or manual setting of 3 measurements, each containing 3 runs at 20 seconds per run were used for sample testing.

2.3.3 MSC culture

Human MSCs were purchased from Lonza. According to Lonza data sheet, mesenchymal stem cells were harvested and cultured from normal human bone marrow. Cells were tested for purity by flow cytometry and for their ability to differentiate into osteogenic, chondrogenic and adipogenic lineages and were also tested positive for CD105, CD166, CD29, and CD44 and negative for CD14, CD34 and CD45. Different lots of MSCs were derived from various donors and therefore were used to exclude donor-dependency. Only passages earlier than 8 were used in this thesis. hMSCs were maintained in defined MSC growth media (MSCGM) (PT-3001, Lonza, Williamsport, PA). In some experiments, serum-free media was used to exclude the inference from the ECM proteins contained in the serum to the Fnf-ANPs. The serum-free media was made by deleting the bovine fetus serum from the MSCGM.

2.3.4 hMSC Adhesion Assay

To test cell adhesion on the nanocarriers, 96-well non-tissue culture dishes were coated overnight at 4℃ with whole-length fibronectin, Fnf or Fnf-ANP. Ligand density of Fnf-ANPs was equivalent to Fnf alone. Wells were washed three times with PBS and hMSCs were seeded in serum-free media with or without the presence of bFGF at 15,000cells/cm^2

and allowed to adhere for 90 min at 37℃. Then the cells were gently washed twice with PBS and the number of cells adhered to surface determined by Hexosaminidase Assay. Briefly, 60μl of substrate (composed of equal volumes of 0.5% Triton X-100 and 7.5mM b-nitrophenyl N-acetyl b-D glucosaminide in 0.1M citrate buffer, pH 5.0) was added to each well and incubated for 90 min at 37℃. After terminating the reaction by the addition of 90μl per well of 50mM glycine/5mM EDTA (pH=10.4), the absorbance was measured at 405nm on a luminescence multi-well plate reader. For antibody blocking control, 1ug/ml anti-integrin α_5 and anti-integrin β_1 (Santa Cruz, USA) were mixed into the cell suspension before cell seeding.

2.3.5. Morphological Studies

8-well Lab-Tek™ Chamber Slides (Nunc, Rochester, NY) were treated with negative oxygen plasma to enhance protein adsorption. (The plasma treatment protocol will be introduced in detail in Chapter 3). 250ul of 40ug/ml of 1) 30nm Fnf-ANPs, 2) 140nm Fnf-ANPs, 3) Fnf and 20ug/ml of 4) WL-FN were added plasma-treated wells and incubated at 4℃ overnight. Then the plates were washed with PBS, blocked with 1% BSA and seeded with hMSCs at 5000 cells/cm^2. Cells were allowed to adhere for 5h at 37℃, then fixed with 3.7% formaldehyde and permeabilized with 0.5% Triton X-100/PBS for 15mins at RT. After blocking in 1% BSA/PBS for 1h at 37℃, the samples were incubated for 1h at 37℃ in 1:400 mouse-anti-vinculin (MAB 3574) diluted in 0.1% Triton X-100 and 10% normal goat serum. After washing, Alexa488-conjugated goat-anti-mouse IgG1 (Invitrogen, USA) was diluted at 1:1000 and added to the samples. After 1h incubation at RT on the rocker, wells were washed

and then incubated with 1:200 Texas Red phalloidin for 30min at RT. Finally, the cell nuclei were stained with Hoechst 33258. Images were taken by the Leica SP2 confocal microscope and analyzed with Image J and Image Pro Plus.

2.3.6 Migration Assays

Two migration assays were performed to evaluate hMSC migration on Fnf-ANPs. First, random cell migration was investigated by seeding isolated hMSCs at the density of 3000-5000 cell/cm^2 onto wells coated with Fnf-ANP, ANP, or Fnf alone. Same as described in the adhesion assay, protein-coated wells were washed three times with PBS and blocked with bovine serum albumin (1 h, 37C). hMSCs were trypsinized and stained with CellTracker™ Green CMFDA (5-chloromethylfluorescein diacetate) (C7025, Invitrogen, USA) at 1:1000 dilution for 20min at RT and washed with serum-free media once. Next, cells were seeded in the wells for 4h to allow them to firmly attach and then transferred to the Leica confocal microscope equipped with a CO_2 chamber for time-lapse live-cell imaging. Three randomly chosen non-overlapping viewing fields were selected in each of the wells and continually imaged at 10X magnification under transmitted light for a total of 12h at10 min intervals. Images were then analyzed with Image Pro Plus (Media Cybernetics, Silver Springs, MD). Time-lapse images were analyzed according to a previously established method by Sharma [39]. The x and y positions of the cell centroid were used to calculate the mean square displacement of the cell tracks based on the following equation: $<d^2>=2S^2P\,[t-P\,(1-e^{-t/P})]$. We observed relatively rapid cell migration in the last 4 hours of the time-lapse study. We

analyzed both the entire migration course as well as the last 4h period and we found the cells migrated significantly and more actively in the last 4h period.

CytoSelect™ 24-Well Wound Healing Assay (Cell Biolabs, USA) was used as an in vitro wound healing model to assess the directed hMSCs migration on Fnf-ANPs. As an alternative of "scratch wound assay", this assay is an easier and more concise method to study wound healing in vitro. As described in Figure 2-1, Fnf-ANPs will be pre-adsorbed at the bottom of each well. MSCs will be seeded in the inserts and cultured until they form a monolayer around the insert. When the insert is removed, a precise 0.9 mm open "wound field" will be left between the cells. Cells can be treated and monitored at this point for migration and proliferation into the wound field.

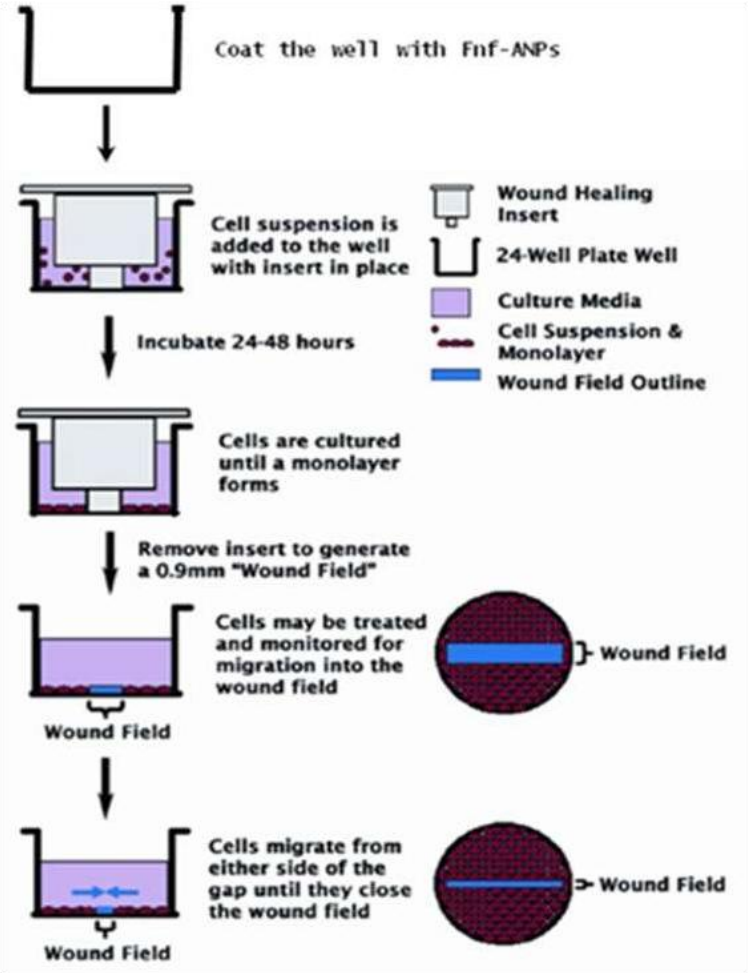

Figure 2-1. Schematic of in vitro wound healing assay (user's manual available on http://www.cellbiolabs.com).

2.4 Results

2.4.1 MSC Adhesion Assay

Given our previous studies of effects of bioactive ANPs on skin cells [29, 39], we extended our investigation to human mesenchymal stem cells, which exhibit a rich diversity of mechanochemically regulated behaviors and show functional responses including adhesion, morphological change and migration toward sites of wound healing. The data on nanoscale

matrix ligand presentation to hMSCs show that fibronectin fragment FNf presentation from ANPs promoted hMSC attachment over that on equivalent concentrations of substrate adsorbed FNf (Figure 2-2). Therefore, the bioactive ANP substrate may be a good platform to investigate how variations in ligand presentation from ANPs may regulate hMSC

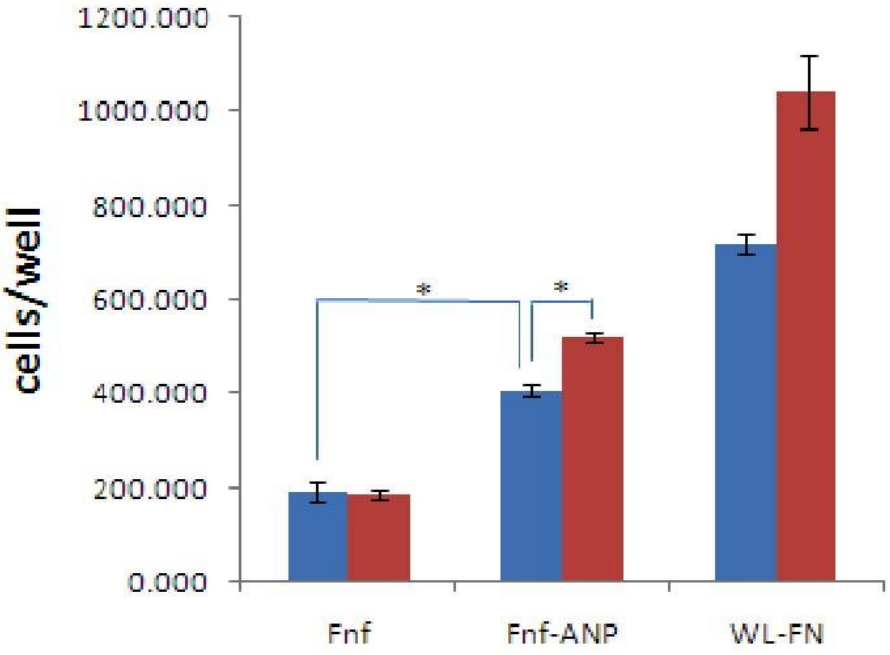

Figure 2-2. ANPs promote hMSC adhesion to $FNIII_{9\text{-}10}$ fragment (FNf) of fibronectin, which is further enhanced in the presence of growth factor (bFGF) (red bars). Each condition has 6 biological repeats and two-way ANOVA in conjunction with Tukey test was used for statistical analysis (* $P<0.05$).

behaviors, and whether these behaviors may be distinctly amplified with growth factor pre-treatment. In vitro cell viability/toxicity assay has shown that surface presentation of the functionalized ANPs to hMSCs enhances cell attachment without compromising cell viability (Appendix Figure A-1,A-2).

2.4.2 MSC Migration Assay

2.4.2.1 Time-lapse Random Migration

To evaluate cellular responses upon longer exposure to Fnf-ANPs, we examined cell migration on Fnf-ANP coated TCPS (Tissue Culture Polystyrene). 24-well plate was adsorbed with Fnf, Fnf-ANP, ANC alone, or WL-FN. The ligand concentration of Fnf and Fnf-ANP was equalized. 20 μg/ml whole-length fibronectin was used as a positive control because it is not only a widely used ECM coating for enhanced cell adhesion and growth but also the mother protein which houses the ligand. Cell migration was conducted with and without addition of bFGF at 20 ng/ml. Our findings show that in the last 4 hours, bFGF enhanced the mean squared displacement in all conditions and it enhanced cell migration on 50nm Fnf-ANPs (bFnf-ANPs) at a larger degree compared to that on 140nm Fnf-ANPs (sFnf-ANPs) (Figure 2-3). Cell migration levels on Fnf were promoted to levels equivalent to whole length fibronectin, when the fragment was presented from the smaller nanoparticles (s-Fnf-ANPs) and in the presence of growth factor (bFGF).

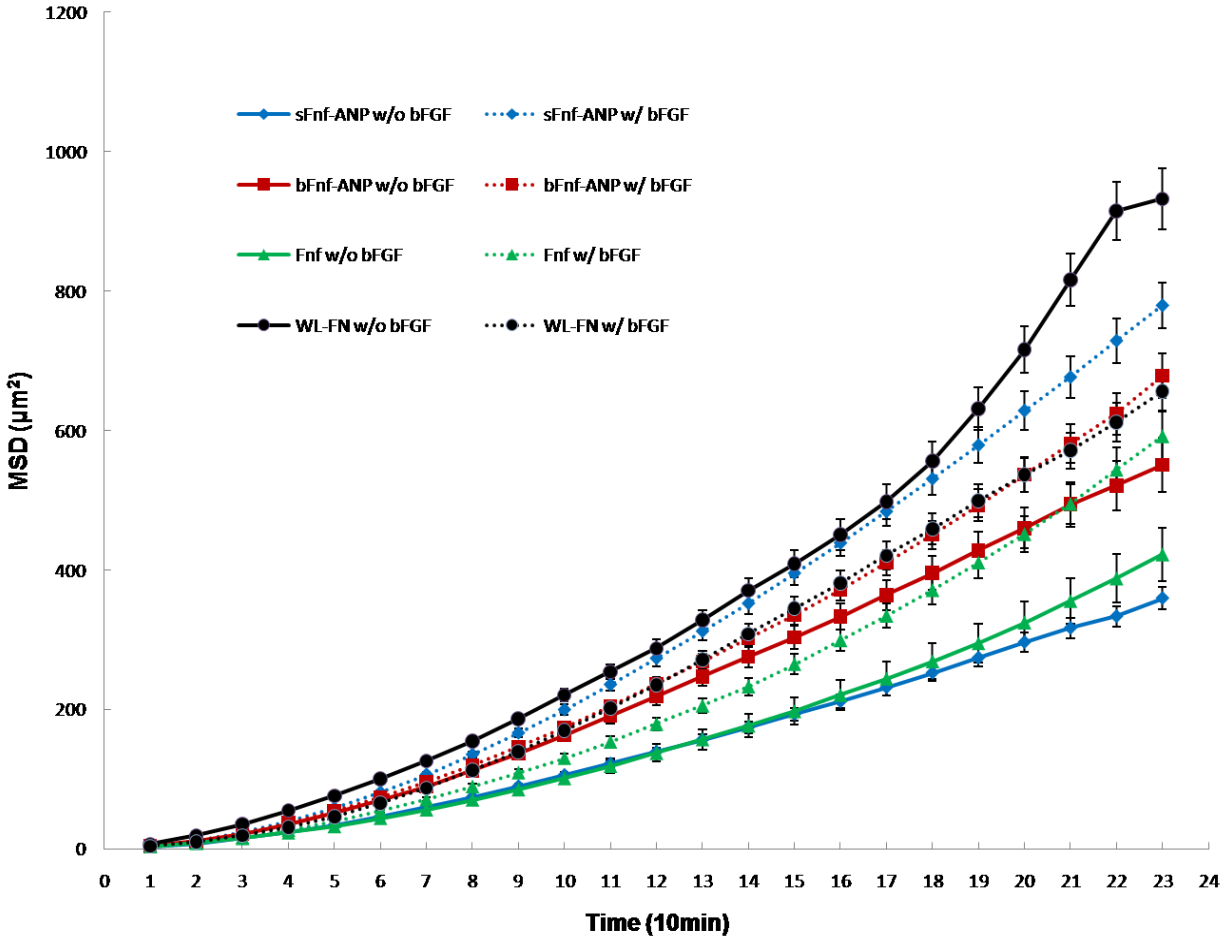

Figure 2-3. Random migration of human mesenchymal stem cells. Single cell migration was examined on substrates with ligand alone (Fnf), unfunctionalized nanoparticles (ANP), and ligand-conjugated nanoparticles (Fnf-ANP) and whole-length fibronectin (WL-FN). hMSCs were seeded at 5000 cells/cm^2 for 4 h prior to image acquisition. Images were taken over 12 h. Only the time points collected in the last 4h were shown here. Error bars represent standard error around the mean. For each condition, around 40-60 cell tracks were analyzed using MATLAB software.

2.4.2.2 In Vitro Wound Healing Assay

Cell motility studies of hMSCs on different sizes of FNf-ANPs versus FNf of equivalent net concentrations was conducted using a CytoSelect™ 24-Well Wound Healing Assay (CBA-120, Cell Biolabs, Inc, San Diego, CA). As an alternative of "scratch wound assay", this assay is a more reproducible configuration to simulate the migration underlying wound healing in vitro. As demonstrated in Figure 2-1, FNf-ANPs, ANPs, Fnf, or WL-FN was pre-

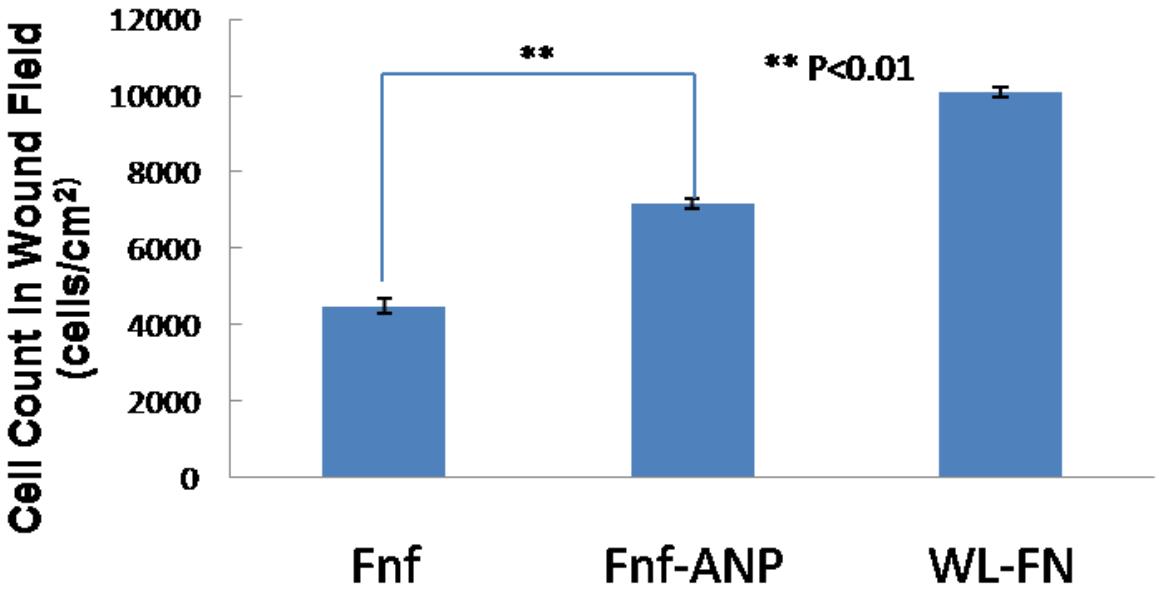

Figure 2-4. hMSC motility kinetics is enhanced on FNf-ANPs relative to Fnf within a 2-D wound healing assay. Positive control: whole length fibronectin (WL-FN). More cells migrated to wound field on Fnf-ANPs that those on Fnf alone ($P<0.01$). 6 fields were counted for each well. Data was analyzed using two-way ANOVA in conjunction with Tukey test for statistical significance.

adsorbed at the bottom of each well. MSCs were seeded in the inserts and cultured until they formed a monolayer around the insert. Cells were allowed to migrate for 24h after insert removal and based on cell count in the wound field, we concluded that Fnf-ANPs promoted

more cell migration to the wound field and therefore has a better effect in healing the "artificial wounds" in vitro (Figure 2-4).

2.4.3 Morphological Observation

hMSCs morphology, cytoskeleton organization and the expression of focal adhesion biomarker--vinculin on two different sized ANPs were compared. Cells appear more dendritic on the small ANPs while they appear more polarized and spread on larger ANPs. Vinculin expression of cells seeded on Fnf or WL-FN seems to be similar—in a pattern of strongly stained puncta distributed in the tips of cell protrusions. While on large-sized Fnf-ANPs, vinculin spreads more universal though the cell body in a long fibrillar pattern. Our early data suggests that hMSCs are sensitive to ANP presentation of an adhesion ligand (Fnf) and this effect is acutely modulated by nanoscale size of ANPs (Figure 2-5).

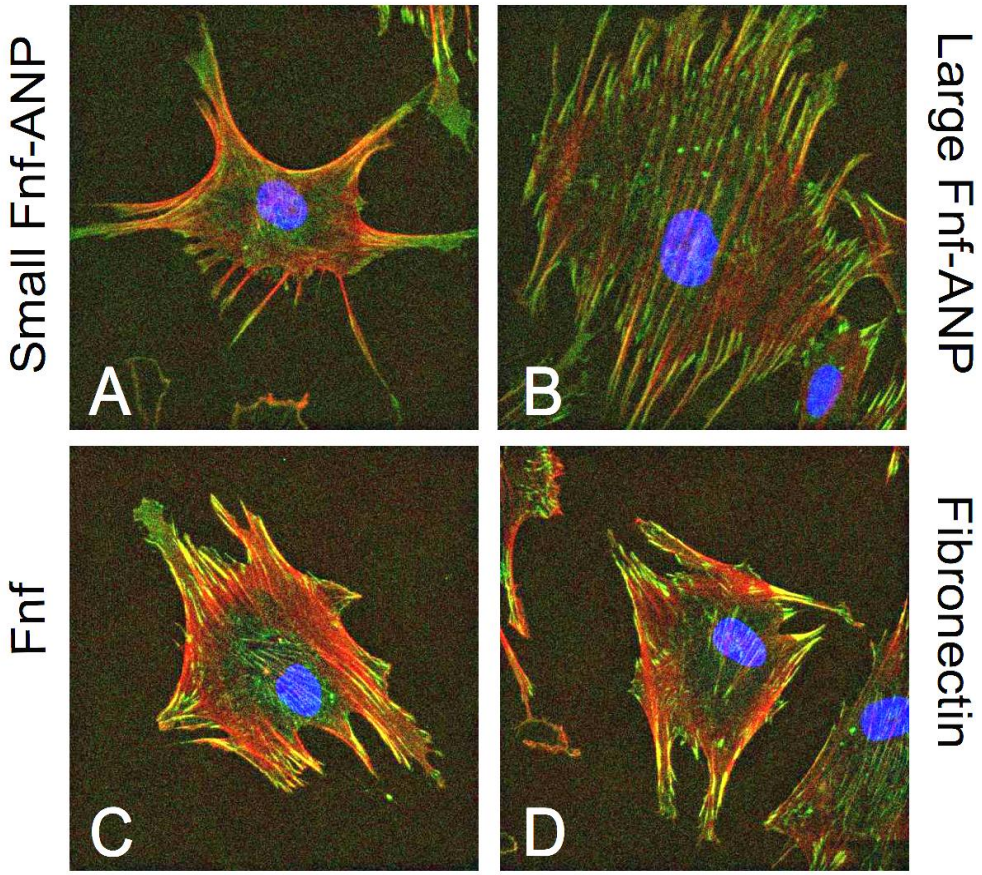

Figure 2-5. Role of Fnf-ANPs on engineering hMSC cytoskeleton organization and vinculin expression patterns. hMSCs change their morphological phenotype (green: vinculin; red: actin; blue: nuclei) on Fnf-ANPs following minute variations in ANP nanoscale size.

2.5 Discussion

The albumin nanoparticle based substrates represent a highly flexible and manipulable nanobiointerface, which could potentially be used to modify biomaterial surfaces in 2-D and scaffolds in 3-D by presenting adhesive ECM-derived ligands specific to a wide range of tissues of interest. Albumin nanoparticle as a carrier for bioactive ligand presentation is attractive because these substrates are highly biocompatible and have prolonged half life in the blood stream. Funded by a NSF Nanoscale Interdisciplinary Research Team (NIRT)

grant, our lab has demonstrated the knowledge of such nanoparticles in skin cell functions [1, 29, 39]. This part of my thesis seeks to provide a basic understanding of ANP effects on hMSC biology and the cell responses within in vitro wound-healing models. We showed that hMSC migration in the wound healing assay was promoted on Fnf-ANPs. We verified that bFGF combination with Fnf-ANPs promoted cell adhesion whereas non-nanoparticle presented Fnf did not exhibit syngergies with bFGF. This finding suggested that the Fnf-ANP system may be a good model to explore synergistic combination of bioactive ANPs and growth factors, which will enhance hMSC adhesion and migration responses. We also observed hMSCs exhibited different morphologies on different sizes of ANPs, stellate and dendritic on small ANPs while fully polarized and more spread out on large ANPs. The size effect in cell shape control needs to be further investigated. Taken together, the bioactive ANP substrate may be a good platform to investigate how variations in ligand presentation from ANPs of variable nanoscale sizes may regulate hMSC behaviors, and whether these behaviors may be further amplified with the addition of soluble chemoattractants such as growth factors and cytokines deficient in chronic wounds. These findings raised the idea of manipulating hMSC fates using the albumin nanoscale system to display growth factor sequestering peptides for directed stem cell differentiation (Chapter 4).

2.6 Conclusion

In summary, the in vitro studies focusing on the interactions between MSCs and nanoparticles supported and showed that compared with ligand alone, Fnf-ANPs are more bioadhesive to MSCs and the adhesion can be further amplified with the presence of bFGF. In an in vitro wound healing assay, more hMSC migrated to close the wound field on Fnf-

ANP than on ligand. hMSCs morphology and the distribution of focal adhesion plaques on two different sized ANPs were also compared. Cells appear more dendritic on the small ANPs while they appear more polarized and spread on larger ANPs.

CHAPTER 3: PLASMA-MICROPATTERNED ALBUMIN NANOPARTICLES: SUBSTRATES FOR ENHANCED DISPLAY OF CELL-ADHESIVE LIGANDS

3.1 Abstract

Spatial guidance of cells via engineering cell adhesion substrate with biomaterials and bioactive molecules can provide clues on cell functions such as attachment, polarization, migration, proliferation, differentiation and cell-cell interactions [40-42]. To achieve this, most biomaterials to date have been decorated with whole extracellular matrix proteins such as fibronectin, laminin, or collagen, here we demonstrate a novel, relatively easy and widely applicable approach to pattern the ligand-functionalized albumin nanoparticles on non-adhesive, biodegradable polymeric substrates. Our approach involves oxygen plasma-treatment of spatially restricted regions on the polymer-coated glass coverslips. Fnf-ANPs were successfully patterned and used as substrate coatings to elicit adhesion and spreading of hMSCs and human foreskin fibroblasts (HFFs) into arrays over similarly patterned ligands. Patterning of both cell types into the plasma-treated polymer regions was considerably more orderly than with Fnf alone. The underlying mechanism might be oxygen plasma treatment selectively enhances ligand exposure on the functionalized nanoparticles, which subsequently induces ligand receptor clustering on the cell membrane. Our results suggest a new nanotechnology approach to spatially direct cell attachment and growth.

3.2 Background and Rationale

Extracellular matrix proteins and cell-matrix interactions have been shown to play a crucial role in guiding cell fate and control processes such as survival, proliferation, migration and differentiation [43, 44]. Considerable effort has been dedicated to manipulate cell behaviors

by localizing these matrix molecules [41, 45]. To date, new techniques such as microcontact printing [46], dip-pen lithography [47], and photolithography [48] have been used to pattern cells into the shape and morphology as wanted. These techniques are very useful in terms of studying the cell-matrix interaction at the nanoscale regimen over which receptor-ligand interactions occur. For example, by varying the spacing between the RGD-biofunctionalized gold dots, Cavalcanti-Adam et al modulated the clustering of the integrin receptors and found that a critical RGD density is essential for the establishment of mature and stable integrin adhesions, which, in turn, induce efficient cell spreading and formation of focal adhesions [27]. Diverse types of nanoparticles are being explored for decoding the focal adhesion mechanism as they are capable of presenting ligands, proteins and peptides at the nanoscale, mimic ligand clustering and promote integrin clustering to trigger or augment cell functions.

This part of the thesis sought to template biodegradable albumin nanoparticles on biocompatible but non-permissive tyrosine-derived polycarbonates for spatial guidance of both somatic as well as stem cells. The lower nanoparticle adsorption on the untreated polymer is caused by the presence of poly(ethylene glycol), or PEG, which inhibits adsorption. Plasma treatment, however, increases the surface energy and negative charge on the surface of the polymer. The higher surface energy of poly(DTE-co-8% PEG1K carbonate) is indicated by the completely wetting contact angle upon plasma-treatment, in comparison to the contact angle of the untreated polymer of $69 \pm 2°$.

We demonstrate a technique to establish spatially controlled patterns of the albumin nanoparticles on non-permissive polymer films by using microscale Plasma Initiated Patterning (μPIP), which uses oxygen gas plasma to enhance the hydrophilicity of the polymer surfaces, therefore to selectively control and organize cell attachment and spreading. Fnf-ANPs were micropatterned into stripes through μPIP on poly(DTE carbonate)–coated substrates and this method was developed by Dr. Mar á P á Rossi at Moghe Lab. By increasing protein adsorption on the initially non-adhesive polymer through plasma treatment, this platform of micropatterned nanoparticle substrates greatly enhances cell adhesion and morphogenesis to the presented ligands on poly(DTE carbonate-co-8% PEG).

3.3 Materials and Methods

3.3.1 Preparation of Polymer Spin-coated Glass Coverslips

Poly(DTE-co-8% PEG_{1K} carbonate) was selected for patterning studies is because it is biocompatible and repels both protein and cell attachment [49]. Poly(DTE-co-8% PEG_{1K} carbonate) was provided by Dr. Joachim Kohn from NJ center for biomaterial. The polymer was diluted in a 98.5% methylene chloride/1.5% methanol solution (v/v) at 1% w/v. The solutions were then spin-coated at 4,000 rpm by using a spin-coater onto acid pre-cleaned 12mm glass coverslips to form thin films (~100 nm).

3.3.2 μPIP

An elastomeric poly(dimethylsiloxane) (PDMS) stamp with parallel grooves 40-300 μm in width and open at both ends was utilized to selectively expose areas of the polymer surface to oxygen plasma. These sizes were specifically chosen to guide microscale cell attachment and spreading, and confirm the bioadhesive functionality of the nanoparticles. The stamp was fabricated by pouring the base and the cross-linker of Sylgard 184 silicone elastomer kit (Dow Corning, Midland, MI) at the ratio of 10:1 over lithographically created masters. As a result, while some of the substrate is protected by the PDMS stamp, the area under the grooves is exposed to the oxygen plasma. The polymer was treated at 50 W for 60-120s to ensure sufficient oxygen plasma treatment. Figure 3-1 is a schematic illustrating the principle of the μPIP. Nanoparticle solutions were again incubated on the polymer surface after treatment overnight at 4 ℃. Consequently, crossed patterns, as shown in the schematic in Figure 3-1, were obtained, where selected regions were either unexposed, or exposed for 60-120 sec. Single and cross-patterning approaches allowed for the spatial organization of biofunctional nanoparticles into simple and more complex arrays, respectively.

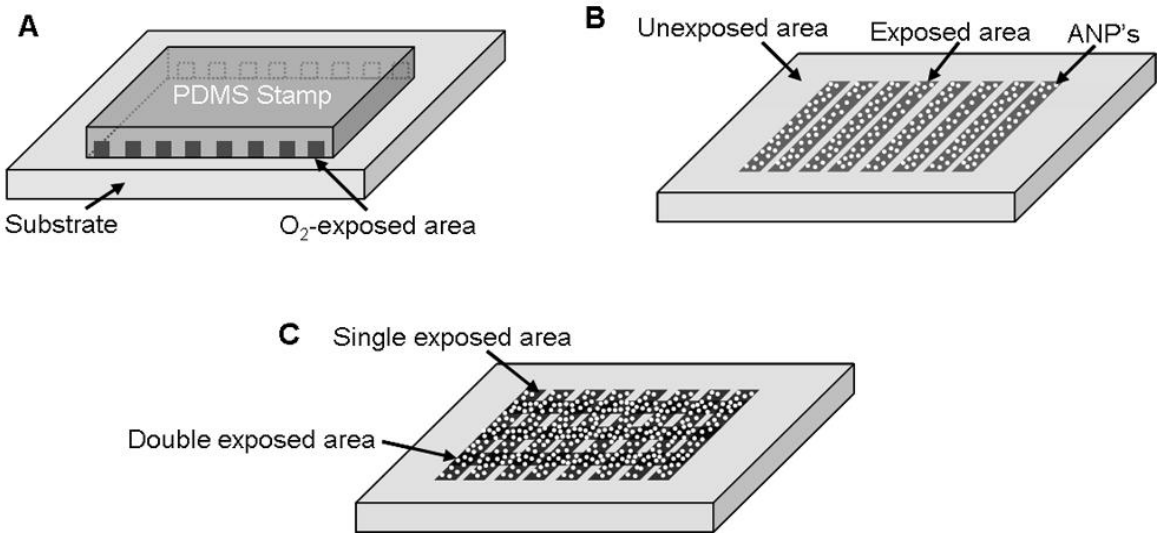

Figure 3-1. Schematic illustrating the microscale plasma-initiated patterning process. (A) A PDMS stamp is placed on the biocompatible, bioresorbable polymer surface and treated in oxygen plasma at a pressure of 660 mTorr for 60-120 seconds and 50 W. Areas of the polymer exposed to the plasma undergo surface functionalization via the formation of end groups by interaction with the radicals, electrons and ions in the oxygen plasma. (B) Biofunctional albumin nanoparticles (ANPs) then preferentially adsorb to the exposed area of the material. (C) By exposing the polymer to the oxygen plasma for 60 seconds, rotating the stamp by 90 ° and exposing the polymer to the oxygen plasma for 60 seconds again, areas of differentially exposed polymer enabled the differential deposition of nanoparticles for cell attachment. (By courtesy of Mar á P á Rossi.)

3.3.3 Fnf-ANP Coating and Cell Seeding

After plasma-treatment, 625ul of Fnf-ANP, Fnf, WL-FN (positive control), or ANP (negative control) solutions were incubated on the plasma-treated polymer surfaces overnight at 4℃ to ensure binding and adsorption of proteins onto the substrates. To pattern hMSCs, stamp templates of sizes ranging from 10μm X 10μm to 200μm X 200μm were prepared as described earlier and washed. Human Mesenchymal Stem cells were trypsinized at 37℃ for 5 minutes, neutralized by MSCGM (Lonza PT-3001) and centrifuged at 600g for 5 minutes. Cells were then counted, diluted to 10,000-30,000 cells/cm^2 and cultured on the Poly(DTE-co-8%PEG1K carbonate) patterned with the biofunctional nanoparticles at a ligand concentration of 2-20μg/cm^2. As a control, patterning of the ligand alone was also done. After plasma-treatment, Fnf stock (with the concentration ~3-5mg/ml) was diluted in PBS to the same concentration and the substrates were incubated with the solution at 4℃ overnight. Similarly, patterning with whole length fibronectin as a control was done for control at a concentration of 10-20μg/cm^2. Substrates were then washed for three times with PBS before cell seeding.

To visualize the organization of nanoparticles into patterns, fluorescent microscopy was employed. Same as before, Fnf-ANP, Fnf, WL-FN and ANP solutions were first incubated on the micropatterned substrates overnight at 4℃. Unbound proteins were washed three times with PBS. Fnf-ANP and ANP samples were incubated with 1:500 FITC conjugated goat-anti-human albumin (Bethyl Laboratories, Montgomery, TX) for 1h at RT. After three washes with PBS, 10min each, the coverglasses were imaged by the Nikon fluorescent

microscope and Leica SP2 confocal microscope. Fnf-ANP and Fnf samples were incubated with anti-Glutathione-S-Transferase (GST) antibody produced in rabbit (G7781, Sigma, St. Louis, MO) at a 1:2000 dilution overnight at 4℃, washed three times and incubated with Cy3 conjugated donkey-anti-rabbit IgG (Jackson Immunolabs, West Grove, PA) at a 1:200 dilution and incubated for 1.5h at RT. The stained patterns were then washed again and stored at 4℃ before imaging. Staining was also performed with the antibodies in the absence of nanoparticles to test for non-specific binding of the antibodies to the micropatterned substrates, and to ensure that the patterns observed were a result of nanoparticle patterning and not antibody patterning (data not shown).

3.3.4 Visualization of Cell Adhesion on Patterned ANPs

Cell seeding on the microscale patterns of the polymer-deposited nanoparticles was assessed by fluorescent labeling of fixed cells after 6 to 24h post-seeding. For staining, cells were washed 3 times with Dulbecco's Phosphate Buffered Saline (DPBS) with Ca^{2+} and Mg^{2+}, fixed with 3.7% formaldehyde for 15 minutes at room temperature, washed, permeabilized with 0.5% Triton X-100 in PBS for 15 minutes at RT and then washed again. Samples were then blocked with 3% calcein (Sigma, St. Louis, MO) for 1 hour. For cytoskeleton staining, cells were incubated with FITC phalloidin at a 1:200 dilution for 30min at RT and washed. Finally, Vectashield anti-fade reagent containing 4',6-diamidino-2-phenylindole (DAPI) (Vector Labs, Burlingame, CA) was used to the samples for nuclear staining as well as to prevent photo-bleaching.

3.3.5 Immunocytochemistry of Integrin α_5 and β_1 Receptors

hMSCs can be spatially patterned onto 100μm wide stripes with 200μm spacing where the FNf-ANPs were specifically adsorbed due to the discontinuous distribution of hydrophilic regions etched by plasma treatment. In the preliminary experiment aimed to study the integrin clustering, cells were seeded in serum-free media and started to form obvious patterns after 16h. The cells were fixed and permeabilized with 0.5% Triton X-100/PBS for 15mins at RT. After blocking, the samples were incubated overnight at 4℃ in mouse anti-human integrin α_5 (isotype: IgG_{2b}, sc-59761, Santa Cruz, USA) and anti-human integrin β_1 (isotype: IgG_1, sc-13590, Santa Cruz, USA), both at 1:100 dilution. After three washes with PBS, Alexa Fluor® 488 conjugated-anti-mouse IgG_{2b} and Alexa Fluor® 594 conjugated-anti-mouse IgG_1 antibodies (Invitrogen, USA) were added to visualize the antigens. Images were taken by the Nikon fluorescent microscope and Leica SP2 confocal microscope.

3.3.6 Quantification of Ligand Exposure

To better investigate the ligand exposure upon plasma treatment on the polymer-coated substrates, we measured its surface adsorption via ELISA. Specifically, anti-GST antibody was used to quantify the differences in protein binding for GST-$FNIII_{9-10}$ between untreated and plasma-treated poly(DTE-co-8%PEG1K carbonate) surfaces. Untreated and plasma treated polymer coverglasses were incubated overnight at 4℃ with either Fnf-ANP or Fnf at different dilutions to avoid over-saturating the substrate. Fnf standards were made by diluting Fnf stock to 20 μg/ml with PBS and making 1:2 serial dilutions. Wells were washed five times with PBS to remove unbound ligand and incubated with blocking buffer (3% non-fat

milk) for 1 h at 37 ℃. After washing five times with PBS, substrates were incubated with rabbit anti-GST (70 ng/mL) (Sigma) for 1 h at 37 ℃. Wells were washed and further reacted with an appropriate HRP-conjugated goat anti-rabbit antibody (1:20,000) (Sigma) for 1 h at 37 ℃. Sigma-FAST OPD tablets (Sigma) were used according to manufacturer's protocol as a substrate for the detection of peroxidase activity. The color reaction was developed for 30 min and absorbance read at 450nm on a multi-well plate reader. The levels of GST-$FNIII_{9-10}$ conjugated to ANC were obtained by linear regression utilizing standard curve of Fnf absorbance.

3.4 Results

3.4.1 Nanoparticle Pattern Characterization

Figure 3-2a shows the stained pattern of the nanoparticles under fluorescence microscopy. The stamp used had a 400μm stripe of exposed area by 100μm of unexposed area; staining of the nanoparticles is observed on the 400μm stripes, indicating that nanoparticles preferentially adsorb to the plasma treated areas and do not adsorb onto the untreated areas. Figure 3-2b demonstrates nanoparticle patterning with Atomic Force Microscopy (AFM). AFM image shows that while nanoparticles form a monolayer on plasma-exposed regions of the polymer, they minimally adsorb to the unexposed areas of the polymer. The patterns were further confirmed with scanning electron microscopy (SEM), shown in Figures 3-2c-e. Figure 3-2c shows two plasma-exposed stripes on which the ANP's preferentially adsorbed, with the unexposed stripes showing no nanoparticle adsorption. A higher magnification image, showing the nanoparticles adsorbed on one of the plasma-exposed stripes, is shown in

Figure 3-2d, with a higher magnification image of the nanoparticles in the stripe shown in Figure 3-2e.

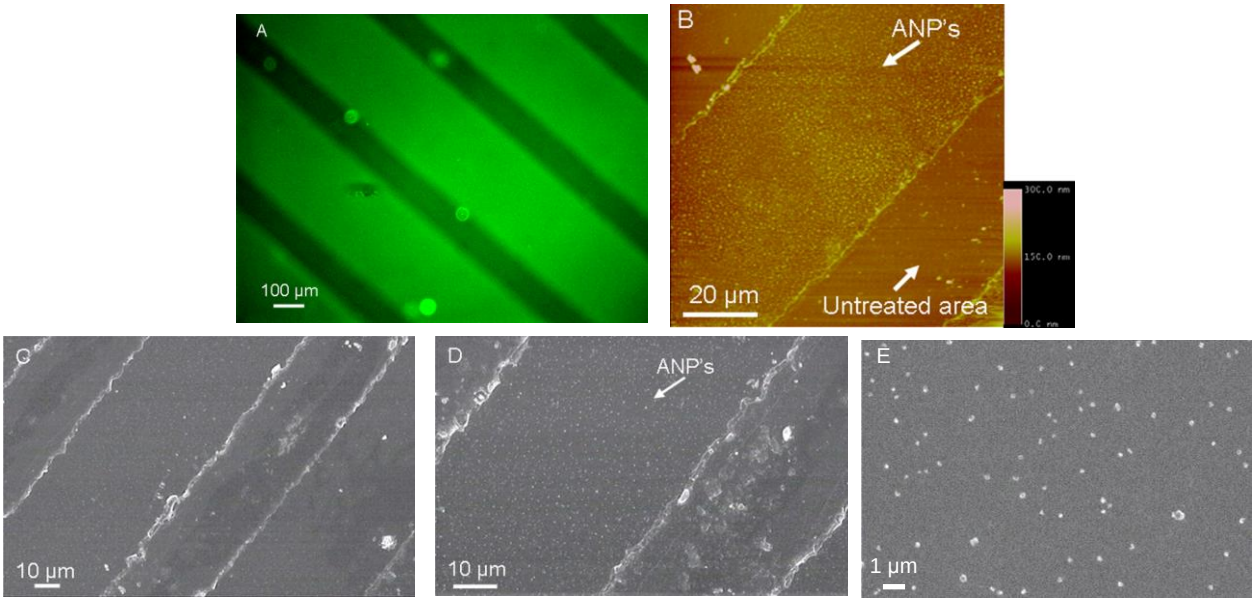

Figure 3-2. Confirmation of spatially restricted patterning of albumin nanoparticles. (A) Fluorescent microscopy image of patterned nanoparticles on Poly(DTE-co-8%PEG1K carbonate). Briefly, after plasma-initiated patterning of the substrate with 660 mTorr oxygen at 50 W for 120 sec, the nanoparticles were adsorbed onto the surface at 4 ℃ overnight, then washed, fixed and stained with mouse anti-human serum albumin as a primary antibody and FITC-Conjugated Donkey Anti-Mouse secondary antibody for visualization under fluorescence. (B) Atomic force microscopy image of nanoparticle patterns on Poly(DTE-co-8%PEG1K carbonate). While nanoparticle monolayers are observed on one of the stripes (the plasma-exposed area), minimal nanoparticle adsorption is observed on the other stripes (unexposed or plasma-protected areas). (C) Scanning electron microscopy image of the nanoparticles patterned on the polymer substrates after plasma treatment. (D) High magnification scanning electron microscopy image of (C). (By courtesy of Mar á P á Rossi.)

3.4.2 Human Mesenchymal Stem Cell Pattern Formation

Cell patterning was also confirmed with the use of human mesenchymal stem cells (hMSCs). Figures 3-4a-b show hMSC patterning with Fnf alone at 4X and 20X magnification. hMSCs

did not form distinct patterned areas, and did not spread evenly within the plasma-exposed areas. When culturing the hMSCs on the Fnf-ANPs, however, well-defined patterns were observed (Figure 3-3c-d), with the cells confined to the plasma-exposed areas yet well spread within these. Interestingly, a similar behavior was observed when full length fibronectin was adsorbed onto plasma-treated polymer surface (Figure 3-3e-f). Thus, by using a small recombinant fibronectin fragment (~50KD) on ANPs, we can functionally mimic its natural whole-length counterpart (~220KD).

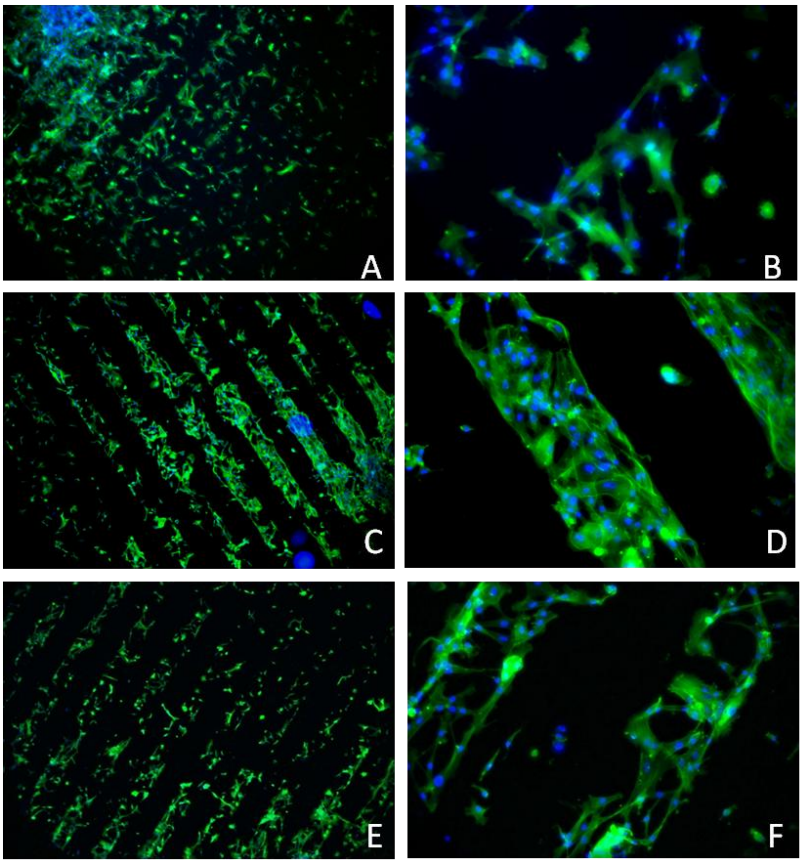

Figure 3-3. Confirmation of spatially restricted patterning of albumin nanoparticles on human mesenchymal stem cells. Fluorescent images of human mesenchymal stem cells (MSCs) patterned with Fnf (fibronectin fragment encompassing the RGD cell binding domain), functionalized albumin nanoparticles and whole-length fibronectin (Green – actin; blue – DAPI). (A) 4X, (B) 20X fluorescent images of MSC's patterned with ligand alone. Patterning is sparse with ligand alone (A), (B). (C) 4X (D) 20X fluorescent images of MSC's patterned with Fnf-ANPs. (E) 4X, (F) 20X fluorescent images of MSCs patterned with whole-length fibronectin (positive control). Patterning with the Fnf-ANPs is more successful than with Fnf alone, and cells clearly spread within the plasma-exposed stripes (C), (D).

3.4.3 Effect of Plasma Treatment on Poly(DTE-co-8% PEG_{1K} Carbonate)

The zeta potential of the unfunctionalized nanoparticles and functionalized nanoparticles were -(11.20±4.59) and -(12.43±2.25), respectively, indicating that their surface charge is

only slightly negative in PBS and that ligand conjugation does not change the surface charge properties significantly. Therefore, the increase in net negative surface charge of poly(DTE-co-8% PEG_{1K} Carbonate) does not considerably repel nanoparticle adsorption; nevertheless, the increase in surface energy and functionalization of the surface diminishes the protein repelling properties of the polymer, promoting adsorption of the nanoparticles to the surface.

3.4.4 Quantification of Fnf Exposure

Ligand adsorption of Fnf and Fnf-ANPs on untreated and plasma-treated poly(DTE-co-8% PEG_{1K} carbonate) was confirmed by ELISA (Figure 3-4). The ELISA data showed that plasma-treatment of the polymer induces greater levels of Fnf exposure on Fnf-ANPs. This data likely indicates that differences in adsorption or binding of the Fnf-ANPs on untreated and plasma-treated surfaces induced differences in exposure of the ligand. As a result, plasma-exposed stripes expose higher ligand density then unexposed stripes, creating the cell patterns in a selective way. With the more uniform substrate coverage by the ligand alone, no cell patterning is induced. The conclusion is oxygen plasma treatment can increase ligand exposure of Fnf-ANPs. The ligand exposure enhancement seems irrelevant to the particle surface charge as both unfunctionalized and functionalized nanoparticles showed similar negative surface charge based on the zeta-potential measurements.

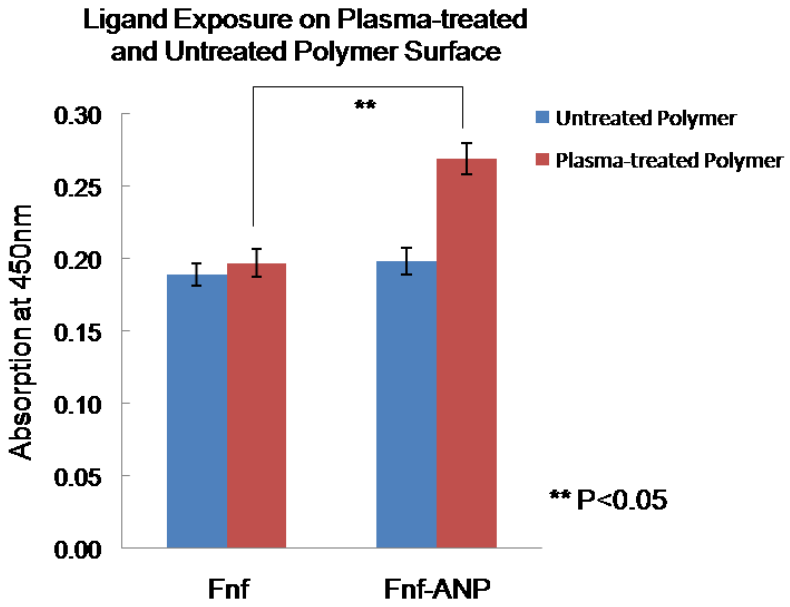

Figure 3-4. Enzyme-Linked Immunosorbent Assay (ELISA) results of the ligand exposure on plasma treated and untreated poly(DTE-co-8%PEG_{1K} carbonate). Oxygen plasma-treatment enhances ligand exposure of functionalized albumin nanoparticles compared to ligand alone. ELISA studies confirm that the Fnf-ANPs exhibit selective ligand patterning on plasma treated substrates, a feature that was exploited to use Fnf-ANPs as carriers to display otherwise non-selective ligand. We adsorbed ligand and FNf-ANPs with net equivalent amounts of ligand on untreated polymer spin-coated glass coverslips. This experiment was repeated twice. No statistical difference in ligand alone adsorption was observed when comparing untreated poly(DTE-co-8%PEG_{1K} carbonate) and poly(DTE-co-8%PEG_{1K} carbonate), while plasma-treated polymer showed an significant increase in ligand exposure on Fnf-ANPs. Student t-test was used for statistical analysis (**P<0.05).

3.4.5 Co-clustering of Integrin $\alpha_5\beta_1$ Receptors on Fnf-ANPs

We also studied the integrin expression pattern on cells seeded on patterned Fnf-ANPs. Using a double immunostaining with two antibodies against integrin α_5 and β_1, we found multiple integrin $\alpha_5\beta_1$ co-stained puncta at the tip of cell protrusions only on cells seeded on

FNf-ANP but not on ligand alone (Figure 3-5). The possible explanation could be that ligand-integrin interaction is concentration-dependent and plasma treatment induced ligand exposure reaches or slightly exceeds the threshold required for integrin receptor co-clustering, while in ligand alone condition, no matter in plasma exposed or non-exposed regions, the ligand concentration is not high enough to induce integrin co-clustering. Another interesting finding is MSCs exhibited different morphologies with Fnf-ANPs and Fnf: stellate and dentritic with FNf-ANPs while fibroblast-like and bipolar with ligand alone. The morphological change could be caused by enhanced ligand exposure or cell remodeling of the albumin particles triggered by nanoscale ligand presentation.

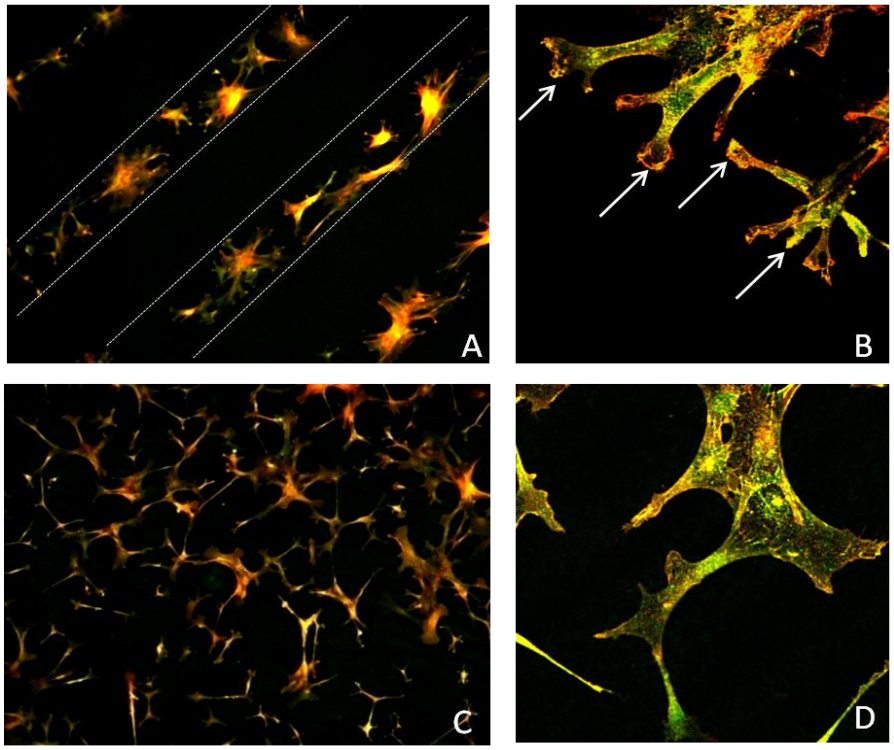

Figure 3-5. Integrin α_5 and β_1 co-cluster at cell peripheries on Fnf-ANPs. μPIP was used to spatially micropattern the functionalized nanoparticles (A, B) and the ligand alone(C, D). Immunocytochemistry images (Green – integrin β1; red –integrin α_5) were taken at 10X (A, C) and 63X (B, D). Note cells only patterned with Fnf-ANPs (dashed lines) but not with ligand alone. Arrow indicates the co-localization of integrin α_5 and integrin β_1 at the tips of pseudopodia with the presence of Fnf-ANPs (B). Interestingly, MSCs exhibited different morphologies with Fnf-ANPs and Fnf: stellate/dentritic with Fnf-ANPs while biopolar with ligand alone.

3.5 Discussion

We developed a platform to pattern organic nanoparticles onto biosynthetic polymers, with the goal of presenting biological cues for selective adhesion of cells. Our platform restricts the deposition of organic albumin nanoparticles within plasma-treated regions on bioabsorbable polymers that have limited levels of hydrophilicity. The spatial treatment, termed as microscale plasma-initiated patterning (μPIP), utilizes oxygen gas plasma to

temporarily modify and functionalize the surface of materials. Functionalization with oxygen gas plasma etches the polymer surface and increases the surface energy of the substrate. Specifically, the ionized gas oxidizes the polymer surface and induces the formation of–COO- and $–CO_3$ functional end groups that render hydrophobic polymers more hydrophilic [50, 51].

Biodegradable, bioresorbable, tyrosine-derived polymers were selected for experiments. Treatment of selected regions of the polymer with the oxygen plasma increases the surface energy and hydrophilicity of the polymer, causing these regions to become adhesive substrates for proteins and protein-based nanoparticles. In the case of Poly(DTE-co-8%PEG_{1K} carbonate), the air-liquid contact angle, measured using goniometry, is 69 ± 2^{o} without treatment. After plasma-treatment, however, the contact angle drops to 0^{o}, indicating a completely wetting surface.

Patterning of cells is of interest for applications in tissue engineering, biosensors and lab-on-a-chip (LOC) devices. Spatially confining cells to various patterns can help provide clues on cellular functions such as attachment, migration and differentiation as well as cell-cell and cell-matrix interactions. However, while patterning with some proteins, such as fibronectin and laminin, has been successful, patterning with smaller ligands derived from whole-length matrix proteins still remains challenging, as shown here with a 50KD fragment of the 220KD long full-length fibronectin.

3.6 Conclusion

We examined the feasibility of establishing biological organization by using organic nanoparticles patterned on non-permissive, biocompatible substrates. In this study, we proposed to use the FNf-functionalized albumin nanoparticles as the key model bionanoparticles for micropatterning studies. By fluorescent, atomic force and scanning electron microscopy, we found that adsorption of ANPs is greater on plasma-exposed polymer in comparison to plasma-protected polymer. ELISA measurements showed that FNf adsorption was not statistically different in plasma-exposed and –unexposed regions of the polymer, while ligand exposure on FNf-ANPs was significantly enhanced in plasma exposed regions than untreated regions. We also found the enhancement of ligand exposure induced by plasma treatment promoted clustering of ligand-specific integrin receptors. Integrin activation has been reported to play an important role in various cell functions including cell adhesion, migration, proliferation and differentiation [24, 52, 53]. Integrin clustering may induce translocation and subsequent stimulation of intracellular signaling, as well as remodeling events related to sequestration and possible internalization of the nanoparticles by the cells, which might explain the different cell morphology on FNf-ANPs compared to FNf alone. Taken together, these results suggest synergistic effects of nanotopography and integrin signaling exerted by ligand presentation on albumin nanoparticles.

Patterning of the Fnf-ANPs allowed for the spatial guidance of hMSCs and HFFs. Both cell types were not only confined to the plasma-exposed areas upon attachment, forming clear

patterns, but they also spread within these regions; when patterning with the ligand alone, patterns of both cell types appeared patchy, and cells did not spread within the exposed areas. In fact, particularly in the case of the hMSC, patterning with the functionalized nanoparticles was comparable to patterning with whole length fibronectin as a widely used ECM protein for cell patterning, demonstrating the usefulness of cell patterning with functionalized nanoparticles.

CHAPTER 4: BIOCONJUGATION OF GROWTH FACTOR SEQUESTERING PEPTIDE ON ALBUMIN NANOPARTICLES

4.1 Abstract

A major challenge to the MSC-based cellular therapy for treating severe chronic wounds is the limited engraftment of these cells at the wound sites [52] and a lack of appropriate stem cell niche for MSC activation and differentiation, which could be solved through optimal combinations of nanoscale adhesive substrates and signaling cues. Growth factors are soluble signaling cues capable of stimulating cellular growth, proliferation and cellular differentiation [53] and they play a key role in tissue regeneration and wound healing [54]. Having demonstrated the application of albumin nanoparticles as a novel nanoscale model system for presentation of adhesion molecules, we sought to extend our ligand type beyond the adhesive ECM peptides and tested the feasibility of conjugating growth factor sequestering peptides (provided by Professor Richard Clark, our collaborator) for enhanced growth factor availability of MSCs. We successfully conjugated the growth factor sequestering peptide (P14) on the 180nm auto-fluorescent albumin nanoparticles made of coacervation method (abbreviated as ANC, in order to be differentiated from ANP made of self-assembly method as described in Chapter 2) and the result was verified by a quantitative measurement of one of the conjugation byproducts, pyridine-2-thione (HPyS). By controlling the ligand/ANC ratio, we were able to quantitatively tailor the ligand presentation density on the particles for various growth factor sequestering purposes in future research.

4.2 Background and Rationale

Wound healing involves multiple cell types, the extracellular matrix and the action of soluble mediators such as growth factors and cytokines. One of the major deficits in severe wounds is the lack of important growth factors [55, 56]. Peptide growth factors and cell surface receptors can be proteolytically degraded in the chronic wound environment. Using dextranomer beads, Cooper et al found the levels of several growth factors were lower or even undetectable in many pressure ulcers [7]. One explanation could be that chronic wounds contain much higher level of matrix metalloproteinases (MMP), which can degrade growth factors much faster than acute wounds [8]. Similar as the ligand-receptor interactions between RGD tripeptide and integrin receptors, the interactions between growth factors and their specific surface receptors also occur at nanoscale regimen. Tremendous effort has been invested in modifying inert biomaterial with growth factors through various techniques including direct covalent immobilization and incorporation of growth factor sequestering ligand such as heparin [57-59]. However, targeting single type of growth factor would be less effective for treating severe wounds compared to targeting a board spectrum of growth factors since chronic wounds are deficit in various growth factors. The laboratory of Richard Clark, MD, our collaborator from the Center for Tissue Engineering at SUNY Stony Brook has isolated growth factor sequestering peptides from the first type III repeat of fibronectin ($FNIII_1$). The largest such peptide was the synthetic peptide FN630-704 from the central 76 residues of $FNIII_1$. Smaller peptides were also isolated: P1: FN634-658, and P2: FN680-704. Both peptides demonstrated binding with PDGF-BB while scrambled variants did not (Figure 4-1). Notably, P1 from $FNIII_1$ could bind $TGF_{\beta 1}$ and bFGF but not to EGF, TGF_{α} and aFGF (data not shown). Further studies with peptides derived from N- and C-terminal trimming

revealed that peptide (P14) FN635-648: PSHISKYILRWRPK is the smallest peptide from $FNIII_1$ with both GF-binding and biological activities. This P14 peptide was used as the key growth factor sequestering peptide for display from albumin nanoparticles in this thesis.

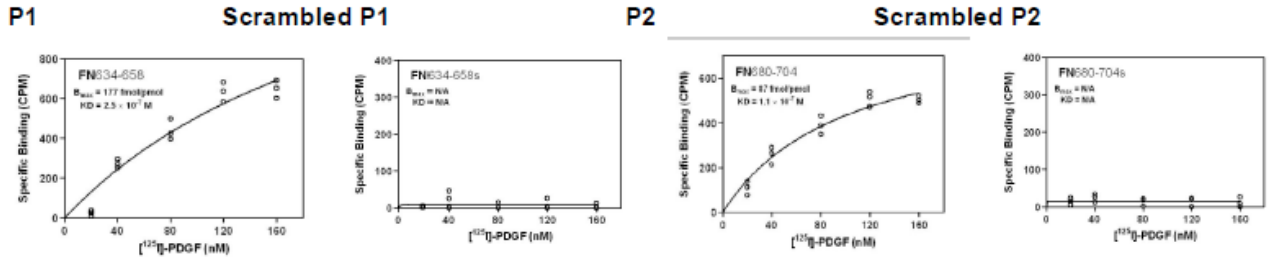

Figure 4-1. Equilibrium binding studies of peptides 1 and 2 (P1, P2) from the two halves of $FNIII_1$ with PDGF-BB. Cys-tagged peptides were conjugated to agarose microbeads via free thiol group according to manufacturer's protocol and incubated with ^{125}I-radiolabeled PDGF-BB in DMEM containing 2% BSA for 2h at room temperature. (By the courtesy of Professor Richard Clark.)

Further, the Clark lab has shown that growth factors bound to $FNIII_{1-2}$ (e.g., $TGF_{\beta 1}$ or bFGF) retain biological activity. $FNIII_{8-11}$ was adsorbed on plastic tissue culture dishes to promote attachment and spreading of human dermal fibroblasts [60] with or without the presence of adsorbed $FNIII_{1-2}$. Fibroblasts cultured in plates coated with both $FNIII_{8-11}$ and $FNIII_{1-2}$ produced type 1 collagen in a dose-dependent manner to increasing concentrations of $TGF_{\beta 1}$ that had been pre-incubated with the FN domain coated plates (Figure 4-2a). No increase in collagen synthesis was observed on plates that were coated with $FNIII_{8-11}$ alone and then pre-incubated with $TGF_{\beta 1}$. Next, fibroblast chemotaxis was performed in response to the GFs in the presence or absence of FN domains. Although $FNIII_{1-2}$ and $FNIII_{12\text{-}V5}$ had no chemotactic activity when assayed alone, they both enhanced the chemotactic activity of

$TGF_{\beta 1}$ (Figure 4-2b), bFGF (Figure 4-2c) and PDGF-BB (Figure 4-2d). In contrast, $FNIII_{3-6}$ did not enhance fibroblast chemotaxis (data not shown).

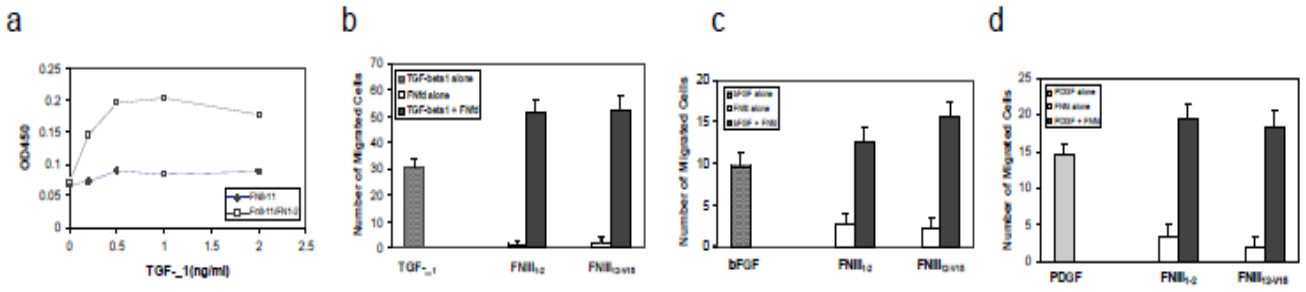

Figure 4-2. $TGF_{\beta 1}$, bFGF and PDGF-BB bound to $FNIII_{1-2}$ and $FNIII_{12\text{-}v15}$ retain biological activity. (a) Collagen levels in medium of cultured fibroblasts. 96-well plates were coated with 100 nM fibronectin domains. After washing, the plates were blocked, incubated with $TGF_{\beta 1}$ and washed. Then, fibroblasts were seeded (1 X 10^4 cells/well) in DMEM containing ascorbic acid, proline, and BAPN. After 24 h, collagen secretion was determined by ELISA. (b) Fibroblast chemotaxis to 0.1 pM (2.5pg/ml) $TGF_{\beta 1}$ in the presence of FN domains. (c) Fibroblast chemotaxis to 5 nM (75 ng/ml) bFGF in the presence of FN domains. (d) Fibroblast chemotaxis to 5 nM (155 ng/ml) PDGF-BB in the presence of FN domains. (By the courtesy of Professor Richard Clark.)

The P14 peptide provided by Dr. Clark lab was modified with a cysteine tag at N-terminal, which can be utilized for conjugation on ANCs. The significance of this work lies in several aspects. First, P14 is a strongly positively charged small peptide, the electrostatic interaction between P14 and the slightly negatively charged ANCs might hinder the covalent conjugation. Therefore, conjugating P14 on ANCs will shed light on the conjugation strategy of small non-neutral peptides on ANCs. Second, the P14-ANCs can be preconditioned with various growth factors or even growth factor cocktails and then induced to cell culture media or as culture substrate to guide lineage-specific differentiation of stem cells. This approach can be developed to a simple, flexible and tunable growth factor sequestering system to study

the stem cells differentiation at nanoscale or to treat diseases with growth factor deficiencies such as severe burns, chronic wounds and many other disorders.

4.3 Materials and Methods

4.3.1 Fabrication of Autofluorescent Albumin Nanoparticles

A coacervation method different than the method mentioned in the second chapter was used to prepare nanoparticles here. An established coacervation technique was used for ANC synthesis from human serum albumin (HSA) monomers [61]. Briefly, lyophilized human albumin (Sigma) powder was dissolved at 2% (w/v) in 10 mM NaCl and the pH was adjusted to 8.50 ± 0.02 with 0.1 N NaOH. Under continuous stirring at 700 RPM at RT, 2 mL of pure ethanol were added by a syringe pump (Harvard Apparatus PHD 2000, Holliston, MA) at 1.5 ml/min to 500µl of the HSA solution in glass scintillation vials. The color of the nanoparticle solution turned from transparent to turbid after ethanol addition. Immediately following ethanol addition, 2.34ul of 8% glutaraldehyde solution was added to crosslink the nanoparticle suspension. Particles were left to crosslink for around 18h under the same stirring rate and at room temperature. On the next morning, ANCs were purified through three rounds of centrifugation (Beckman Coulter, Avanti J-E Centrifuge) at 16,100 g for 8 min at 4℃ in pre-chilled chamber. Each run of centrifuge was followed by washing and redispersion of the pellet to the original volume (2ml) with PBS. Redispersion was performed by vortexing the particles at maximum speed for 10 seconds and followed by sonication (Fisher Scientific, FS60) for 15min.

4.3.2 Physical Characterization

ANCs were studied using DLS and SEM. As introduced before, particle size distributions and polydispersity indexes (PDI) were determined using a Malvern Zetasizer Nano (Zen 3690, Malvern, Worcestershire, UK). Samples were diluted 1:10 in PBS for all the measurements. Z-average sizes and polydispersity indexes of three sequential sample scans (automatic settings) were measured at 25℃. ANCs were visualized using scanning electron microscopy, SEM (JEOL 2010F or AMRAY 1830I), operated at 5-20 kV. 50µl of nanoparticle solution was deposited on 12-mm pre-cleaned glass coverslips and air dried in the tissue culture hood overnight at RT. On the next day, the coverslips were collected and sputtered for SEM.

4.3.3 TNBS Assay

Primary amino group contents on nanoparticles were determined using a colorimetric assay with 2,4,6-trinitrobenzenesulphonic acid (TNBS) [62]. Briefly, The purified ANCs were dissolved at 1:5 to 1:20 (20-200 µg/ml) in 0.1 M sodium bicarbonate buffer (pH 8.5) and 0.5% TNBSA stock solution was also diluted 500-fold in 0.1 M sodium bicarbonate buffer (pH 8.5). Then 0.5 ml diluted TNBSA solution was mixed to 1 ml of protein solution and incubated at 37℃. After 2h incubation, 0.5 ml of 10% SDS and 0.25 ml of 1 N HCl were added to each sample to stop and stabilize the reaction. The mixture was then centrifuged at 16,100 g for 8 min at RT to pellet ANCs. 600ul supernatant was collected and plated to each well in triplicates at 200ul/well on a UV-bottom 96 well plate. The absorbance of solutions was measured by a plate reader at 335 nm. Standard curve was made by 1:2 serial dilution of

glycine in sodium bicarbonate buffer with the starting concentration at 20 μg/ml. The standard curve was plotted in Excel and the concentration of free amine groups on ANCs was quantified.

4.3.4 Preparation of P14-conjugated ANCs

P14 peptides were attached to the ANCs through a standard protein cross-linking protocol with Sulfo-LC-SPDP. Briefly, nanoparticles were resuspended in PBS-EDTA (PBS with 1 mM EDTA and 0.02% sodium azide, pH 7.5) at the final stage of purification. 1 mM of Sulfo-LC-SPDP was introduced to 2 mg of nanoparticles for 30 minutes at RT under agitation (Figure 4-3). For quantification analysis, DTT was used to reduce the SPDP-albumin nanoparticles to yield the byproduct pyridine-2-thione (HPyS) group. HPyS can be measured at its characteristic absorbance of 343 nm to estimate the amount of P14 conjugated on ANPs. P14 was added and reacted with the SPDP-ANC at different ratio (P14: SPDP-ANC=1:4-1:2) for 2 hours at RT. Products were purified through centrifugation and redispersed in PBS, as described before.

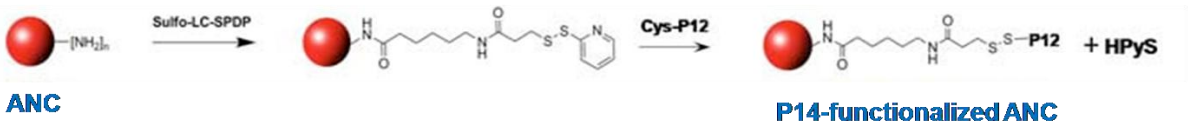

Figure 4-3. Schematic of P14-ANC bioconjugation processes.

4.4 Results

4.4.1 Characterization of Autofluorescent Albumin Nanoparticles

DLS data showed that the average size of unfunctionalized ANCs is 181.23±1.17 nm with the PDI around 0.116±0.023 (Table 4-1). After P14 conjugation, the nanoparticle system became too polydispersed to be measured with PDI varying from 0.5 to 1. DLS also showed the functionalized nanoparticles are not stable in the PBS solution, given sample size exceeds upper limit (100000.0 d.nm) and the polydispersity index is very high (0.5~1.0). Therefore, nanoparticle morphology may change after conjugation and the size distribution is very polydisperse and may not be suitable for DLS measurements. Samples contain large particles/aggregateds/dust. Unfunctionalized ANCs displayed strong, green emission when excited with 488 nm light (data not shown) [63].

Particle Type	Average Size (nm)	PDI
ANC	181.23±1.17	0.116±0.023
P14-ANC	multiple peaks	>0.5

Table 4-1. DLS data of unfunctionalized and P14-functionalized nanoparticles. P14-ANCs have much higher polydispersity index (PDI) than unfunctionalized ANCs, indicating sample contains large aggregates and the particle size does not remain homogenously spherical after conjugation.

Scanning electron microscopy observations confirmed with DLS results that unfunctionalized ANCs display monomodal size distribution (Figure 4-4), while P14-ANCs cluster into large microscale aggregates and exhibit various morphologies with single P14-ANC still remains spherical. This explains the multi-peak size distribution and huge PDI of P14-ANC measured by DLS: P14-ANCs aggregated beyond the measuring capabilities of DLS when dispersed in PBS.

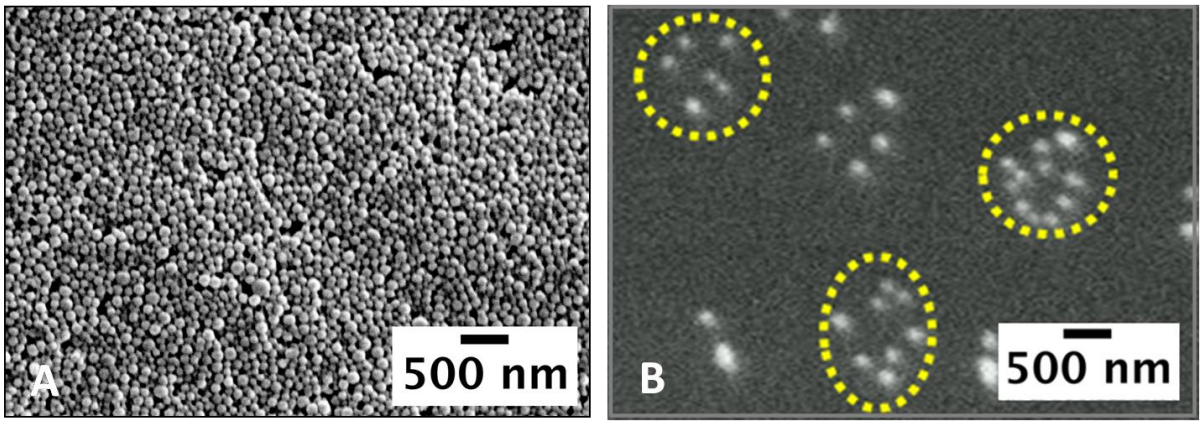

Figure 4-4. SEM images of unfunctionalized and P14-functionalized nanoparticles. Unfunctionalized albumin nanoparticles (ANCs) are monodisperse (A) while P14-functionalized ANCs cluster into aggregates of various morphologies and sizes, as shown in yellow dashed circles (B). (Figure A by courtesy of Dominik J. Naczynski.)

4.4.2 TNBS Assay

Trinitrobenzene sulfonic acid (TNBS) has been used as a hydrophilic modifying reagent for the detection of primary amines in samples containing free amine groups. It is an excellent reagent for rapid qualitative and quantitative estimation of these biomolecules. TNBS reacts readily with the primary amino groups of amino acids in aqueous solution at pH 8 to form

yellow adducts. The colored derivatives are monitored at 335 nm. Using glycine as the standard to react with TNBSA gave us a standard curve of protein concentration against the OD value at 335nm with the square of the correlation coefficient as high as 0.9998 (Figure 4-5) . By TNBS assay, the concentration of free amine groups on ANCs is determined at 0.159 umol/ml or 0.159 mM/L.

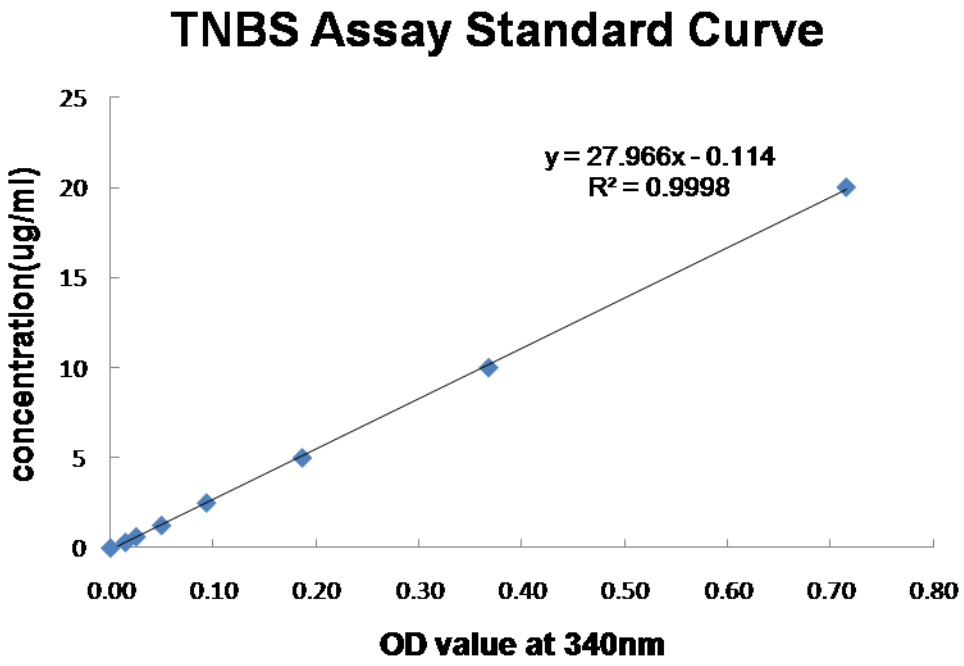

concentration (µg/ml)	MW of Glycine (g/mol)	free amine groups (µmol/ml)
11.911	75.070	0.159

Figure 4-5. Unfunctionalized ANCs contain 0.159 umol/ml free amine groups based on the TNBS assay result. Glycine (MW=75.07) was used as the standard with one free amine group per molecule. The standard curve was made by 1:2 serial dilution of glycine in 0.1 M sodium bicarbonate buffer starting at 20 µg/ml. All eight concentrations was plotted against the optical absorption values at 335 nm. Samples were diluted at 1:5, 1:10 and 1:20 for TNBS reactions and the final concentration was determined at 0.159 µmol/ml.

4.4.3 Bioconjugation Reaction Characterization

ANCs were functionalized with P14 peptides using a standard cross-linking procedure conjugating the free amine groups on the albumin particles to free thiol groups present in the N-terminal cysteine on the ligands. The 1:1 stoichiometric reaction resulted in the generation of pyridine-2-thione, a detectable byproduct that can be quantitatively measured to estimate the degree of ligand conjugation. 244 μg of reactive free amine groups on ANCs and increasing amounts of sulfo-LC-SPDP (32.2 or 64.4 μg) were incubated together to effect the conjugation of PD groups to 25% or 50% of the total free amine groups on the surface of the nanoparticles. In order to estimate the actual conjugated PD groups on ANCs, DTT was added to ANC-PD and based on the number of uM of HPyS (byprodect) generated, we speculated the amount of P14 can be conjugated to the surface of the ANC-PD. Generally, for the purpose of maximizing the P12 exposure, we used 3 fold of P14 to react with the maximum available PD groups with the DTT reaction. After the conjugation reaction between P14 and ANC-PD, we purified the P14-ANC by centrifugation and saved the first and last supernatant for HPyS measurement again. Based on the amount of HPyS generated from the conjugation process, only by varying the SPDP, we obtained P14 concentration on the functionalized ANCs at 5.43 μM in the 25% reaction condition and 11.13 μM in the 50% reaction, which is around two-fold of the 25% reaction (Figure 4-6). Therefore, by varying the cross-linker concentration we were able to control the ligand exposure on the ANCs for further functional studies using the cell-based assays.

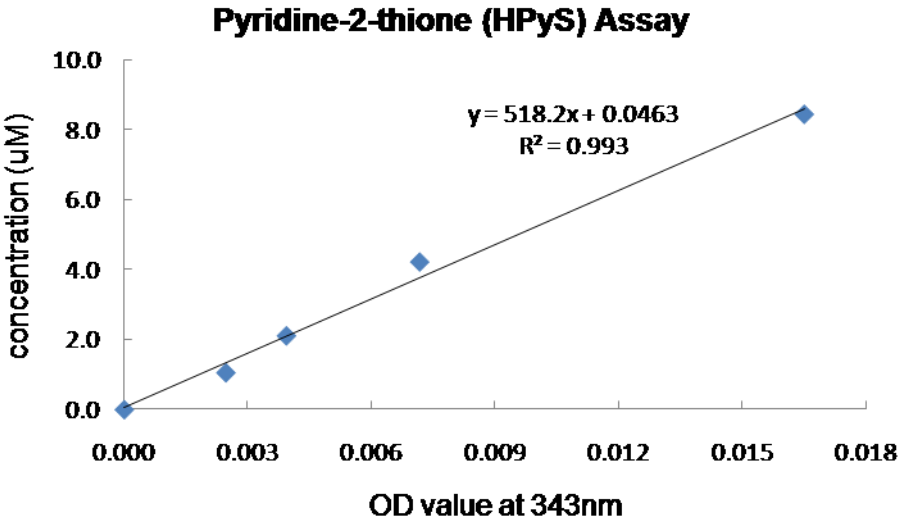

(SPDP/-SH)*100%	concentration (uM)
25%	5.430
50%	11.182

Figure 4-6. Pyridine-2-thione (HPyS) assay. Based on the amount of HPyS generated from the reaction of ANC-PD and cys-P14, we obtained 5.43 μM P14 conjugations in the 25% reaction and 11.13 μM in the 50% reaction, indicating the feasibility of quantitative control of ligand exposure through varying the amount of cross-linker added before conjugation.

4.4.4 Poly-D-Lysine Treatment

As a positive charged biocompatible coating material, poly-D-Lysine (PDL) has been widely used as coatings for in vitro cell culture substrates, biosensors, spinal cord implant and so on. Poly-L-Lysine has been reported to be used as a coating material for albumin nanoparticle preparation and shown to increase the zeta potential of the uncoated nanoparticles from -26mV to -16mV [64]. Here, we used poly-D-Lysine to break up the nanoparticle aggregates. As shown in Table 4-2, after PDL coating, the average size of functionalized ANCs (P14-

ANCs) dropped to 229.17±3.18 nm with PDI around 0.31. The size decrease was verified by SEM (data not shown).

Particle Type	Average Size (nm)	PDI
ANC	181.23±1.17	0.116±0.023
P14-ANC	multiple peaks	>0.5
P14-ANC + PDL	229.17±3.18 **	0.31±0.045

Table 4-2. Coating of ANCs with PDL. P14-ANC solution was divided into two parts, one treated with PDL and one without. 50 μg/ml PDL was added to P14-ANCs and mixed together for 1h at RT on the shaker. After incubation, the pretreated P14-ANC was sized immediately. P14 conjugation and PDL coating increase ANC size significantly, comparing the average ANC size at 181.23 nm with the average P14-ANC size (coating with PDL) at 229.17 nm (** $P<0.01$).

4.5 Discussion

Nanoparticles derived from human albumin have been widely proven to be biocompatible and bioabsorbable with many cell types [65, 66]. The advantages of drug delivery by albumin particles involve low or no immunogenicity and long half-life and stability in serum [61, 67, 68]. Albumin-derived nanoparticles have adequate functional groups such as free amines, carboxyls and thiols, which can be utilized to conjugate ligands, antibodies and other peptides [1, 29, 69, 70]. Naczynski and Andelman from Moghe lab have successfully functionalized albumin nanoparticles with cyclic arginine-glycine-aspartic acid (cRGD), a

tripeptide specifically targets $\alpha_V\beta_3$ integrin receptors on cell membrane [63]. Adopting their methodology, a growth factor sequestering peptide was conjugated to the autofluorescent albumin particles made via the same coacervation method. The unfunctionalized nanoparticles developed and presented here exhibit narrow size distribution, while after conjugation with P14, they aggregate into microscale clusters with very high polydispersity index (PDI~1.000). Poly-D-Lysine was as a coating material to increase the negative zeta potential of albumin nanoparticles. 50 μg/ml was reported to successfully break up the P14-ANC aggregates and decrease the average size of functionalized particles down to 230nm. Based on TNBS and HPyS assays, we verified the successful functionalization of P14 to the ANCs through a standard protein cross-linking protocol with Sulfo-LC-SPDP. P14-ANCs can be used in the future to engineer stem cell phenotype and control lineage commitment as a novel bionanotechnology approach.

4.6 Conclusion

We successfully functionalized a growth factor sequestering peptide P14 to the ANCs through a standard protein cross-linking protocol with Sulfo-LC-SPDP. For quantification analysis, byproduct pyridine-2-thione (HPyS) was measured at its characteristic absorbance of 343 nm to estimate the amount of P14 conjugated on ANPs. Primed with different combinations of various growth factors, P14-ANCs can be applied towards enhanced signaling and differentiation of stem cells or precursor cells for tissue regeneration.

CHAPTER 5: FUTURE DIRECTIONS

A novel nanobiotechnology method utilizing biofunctionalized albumin nanoparticles for enhanced human mesenchymal stem cell adhesion, spatial guidance and growth factor availability was developed. The significance and goal of this study is to advance scientific understanding of how nanoscale biofunctionalized particle-based substrates regulate stem cell functions. Specifically, the future direction will focus on exploring the capability and flexibility of this biointerfacial system in displaying various nanoscale adhesive and signaling cues and identifying the nanoscale determinants of stem cell responses critical to chronic wound repair. We have demonstrated that we can successfully conjugation the growth factor peptide P14 on ANCs, the next step would be investigate the binding efficiency of P14-ANCs to various growth factors and identify the one or two combinations that will accelerate hMSC differentiation to skin cell lineages (epithelial cells and myofibroblasts/fibroblasts). Researchers have combined nanoscale ECM presentation and soluble growth factors to control cell shape, survival, proliferation, migration and differentiation [59, 71]. It has been shown that integrin and receptor tyrosine kinases (receptors bind to a big variety of growth factors), co-clustered by FAK, collaborate synergically to regulate cell functions [72, 73]. Therefore, if Fnf-ANPs and P14-ANCs exhibit synergistic effects in targeted MSC differentiation towards skin cell lineages, a sequential functionalization method can be used to fabricate “bi-functional” albumin nanoparticles displaying both RGD-containing adhesive ligand and FNIII1-derived non-adhesive but growth factor sequestering peptide (GFSP or P14), as demonstrated in the schematic below (Figure 5-1). Based on this model, we hypothesize nanoscale presentation of both ligands on ANPs might promote crosstalk between the integrin- and receptor tyrosine

kinase-related signaling pathways and elicit enhanced cell functions to a higher degree than single ligand presentation. We will explore the synergistic presentation of matrix adhesion ligands and growth factor sequestering peptides from nanoscale ANPs, and investigate the concerted effects on hMSC responses in vitro and in vivo.

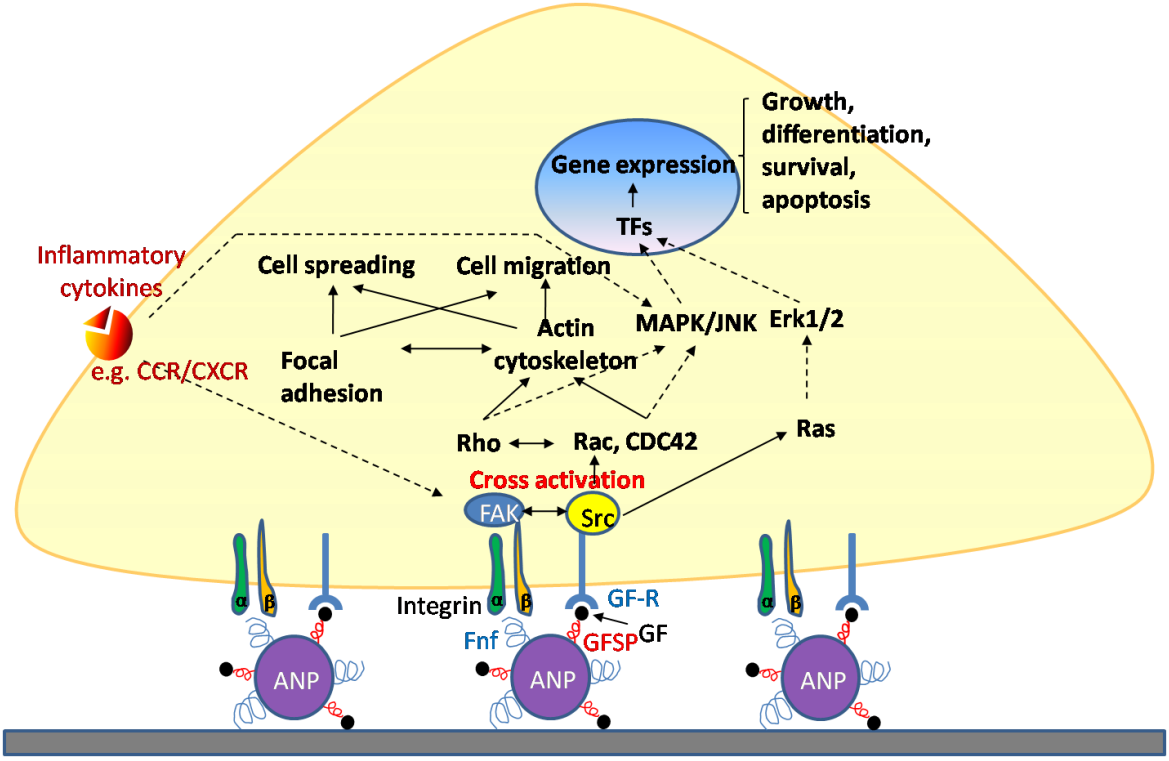

Figure 5-1. Cartoon depicting the possible synergistic cooperation of $FNIII_{9\text{-}10}$ and $FNIII_{1}$-derived growth factor sequestering peptide (GFSP, or P14) based on bifunctional ANPs of varying nanoscale sizes. GFGFR/GF-R and $FNIII_{9\text{-}10}$/integrin binding have intracellular cross-talk. Differential "activation" by chemokines (e.g., CXCL5, simulating later stage inflammatory signals), or early inflammatory factors like TNF-a, IL8, etc. can further amplify RAK signaling pathways. Finally, Different sized ANPs may further alter the Rho/ROCK based cytoskeletal signaling and lineage outcomes. We expect to determine the effects of bi-functional (adhesion & growth factor presenting) ANPs of different sizes on behaviors of differentially activated hMSCs.

The other direction we will pursue with this project is to incorporate ANPs in 3-D synthetic microscaffolds and use the composite for hMSC delivery to wound sites to achieve enhanced clinical outcome. For the polymer substrate, we have been utilizing synthetic tyrosine-derived polycarbonates selected from a library of combinatorially designed polymers, developed by Professor Joachim Kohn at the New Jersey Center for Biomaterials [49, 74-79].

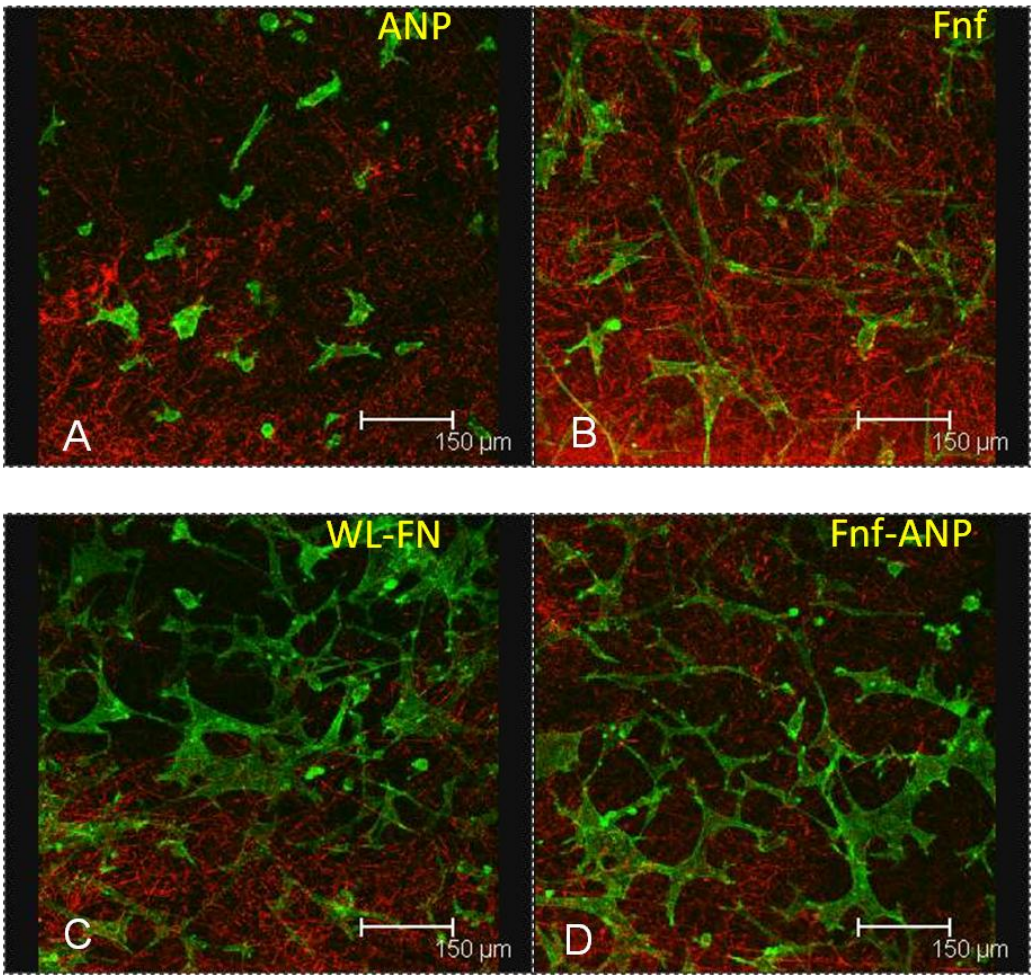

Figure 5-2. hMSCs show dendritic morphology within Fnf-ANP decorated 3-D synthetic scaffold. Scaffolds were incubated with Fnf (B), WL-FN (C) and Fnf-ANP (D) overnight at 4 ℃ to promote adsorption onto the surfaces of the scaffold fibers. As a control, unfunctionalized ANP was adsorbed (A) and this scaffold showed very limited cell attachment, and cells did not spread on the fibers.

We have fabricated a poly(DTE carbonate) scaffold by electrospinning method and to modify the internal fiber surface with bioactive ANPs (data not shown). Tyrosine derived polycarbonates were chosen as the scaffolding material due to their biocompatibility and ability to biodegradable in a controllable manner. hMSCs attached to FNf-treated scaffolds and appeared to spread along individual fibers (Figure 5-2B). In contrast, FNf-ANP treated scaffolds showed enhanced cell attachment with cells spread among the fibers and forming cell-cell contacts. Interestingly, a similar behavior was observed when full length fibronectin was adsorbed onto fibers (Figure 5-2C). Thus, by using a small recombinant fibronectin fragment (~50KD) on ANPs, we can functionally mimic its natural whole-length counterpart (~220KD). This engineered 3-D bioactive "microniche" for hMSCs will be screened in vitro to examine the roles of three key parameters: nanoparticle size, fiber geometry, and ligand selection on functional behaviors of hMSCs. We will also deliver GFP-labeled MSCs within these ANP-based 3-D scaffolds to a full-thickness wound healing model using db/db diabetic mice and investigate how the transplants affect the wound healing processes in vivo.

APPENDIX

Biocompatibility Assessment of Fnf-ANPs

Biofunctionalized albumin nanoparticles were also shown to be biocompatible by biocompatibility assay using human primary fibroblasts as well as skin testing in normal BALB/c mice.

LIVE/DEAD® Viability/Cytotoxicity Kit for mammalian cells (Invitrogen, USA) was used for biocompatibility test of the nanoparticles and the ligand on human foreskin fibroblasts (HFFs). HFFs were typically grown in 10% serum-containing medium for 3 days with the starting seeding density 5000cells/cm^2 until they reached subconfluency. Fnf-ANP, Fnf and ANP were added to the culture media, respectively. After 24h treatment, cells were stained with calcein AM and ethidium homodimer-1 (EthD-1). Every condition had 6 biological repeats. We analyzed data using two-way ANOVA in conjunction with Tukey test and we considered results statistically significant only when $P<0.05$. LIVE/DEAD® Viability/Cytotoxicity assay using human primary skin fibroblasts showed the viable cells accounted over 90% of the whole population, indicating Fnf-ANPs are biocompatible (Figure A-1).

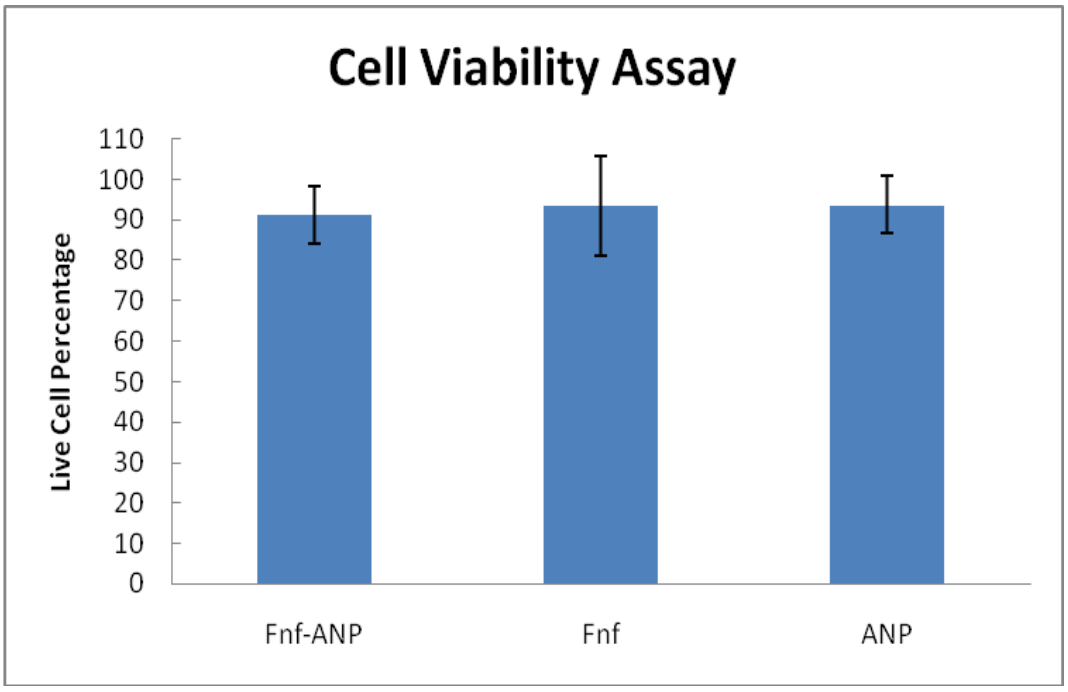

Figure A-1. In vitro viability assay of unfunctionalized and functionalized nanoparticles.

For in vivo biosafety assessment, a skin test was conducted by intradermally injecting Fnf-ANPs in the back skins of normal BALB/c mice (Male, 3-4 weeks of age, 12-15g of weight, obtained from Taconic Farms Inc, USA.). Animals were housed in facilities at Nelson Laboratories, Rutgers University. The facilities are AAALAC certified and operate under the supervision of veterinary staff. Animals were handled in strict compliance with procedures set forth in "The Care and Use of Laboratory Animals" (NIH Publication No. 86-23) to make sure they experienced minimal pain or discomfort. Animals were anesthetized with an intraperitoneal injection of 240 mg/kg Avertin (2, 2, 2-Tribromoethanol) and then the skin of the back was shaved with an electric clipper (Papaioannou and Fox 1993). 50µl of 1) PBS, 2) ANP, 3) Fnf-ANP or 4) Fnf was injected intradermally in each site with a 31-gauge needle from an insulin syringe (sample size n=6). After injection, they were transferred back to their

cages and monitored every other day. After 3 days, the animals were sacrificed and the skin injection sites were excised by sharp scissors. Skin samples were fixed in 4% formaldehyde for 4h at RT and transferred to 30% sucrose solution and stored at 4 ℃ until they sank. Fixed skin samples were embedded in OCT embedding medium and sectioned into 6-10 um slices. Hematoxlin and eosin (HE) staining was performed and the slides were dehydrated in a gradient of ethanol and followed with clearing step in xylene overnight. Images were taken at 20X magnification with contrast microscopy (Nikon Eclipse TE2000-S). In vivo skin test also proved that albumin nanoparticles are biosafe as given by no inflammation was found in Fnf-ANP, Fnf or ANP injected skin samples (Figure A-2).

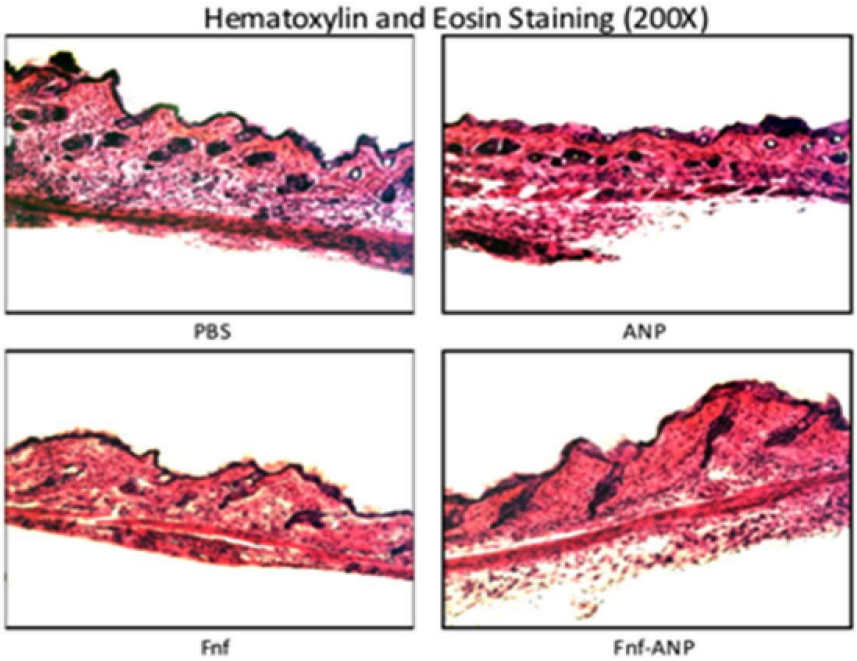

Figure A-2. ANPs are highly biocompatible and do not elicit any inflammatory response 3 days after intradermal injections in BALB/c mice. H&E staining confirms the lack of inflammatory cells at site of injection.

REFERENCES

1. Sharma, R.I., D.I. Shreiber, and P.V. Moghe, *Nanoscale variation of bioadhesive substrates as a tool for engineering of cell matrix assembly.* Tissue Eng Part A, 2008. **14**(7): p. 1237-50.
2. Jones, K.R., K. Fennie, and A. Lenihan, *Evidence-based management of chronic wounds.* Adv Skin Wound Care, 2007. **20**(11): p. 591-600.
3. Moreo, K., *Understanding and overcoming the challenges of effective case management for patients with chronic wounds.* Case Manager, 2005. **16**(2): p. 62-3, 67.
4. Menke, N.B., et al., *Impaired wound healing.* Clin Dermatol, 2007. **25**(1): p. 19-25.
5. Yager, D.R., R.A. Kulina, and L.A. Gilman, *Wound fluids: a window into the wound environment?* Int J Low Extrem Wounds, 2007. **6**(4): p. 262-72.
6. Wallace, H.J. and M.C. Stacey, *Levels of tumor necrosis factor-alpha (TNF-alpha) and soluble TNF receptors in chronic venous leg ulcers--correlations to healing status.* J Invest Dermatol, 1998. **110**(3): p. 292-6.
7. Cooper, D.M., et al., *Determination of endogenous cytokines in chronic wounds.* Ann Surg, 1994. **219**(6): p. 688-91; discussion 691-2.
8. Trengove, N.J., et al., *Analysis of the acute and chronic wound environments: the role of proteases and their inhibitors.* Wound Repair Regen, 1999. **7**(6): p. 442-52.
9. Cowin, A.J., et al., *Effect of healing on the expression of transforming growth factor beta(s) and their receptors in chronic venous leg ulcers.* J Invest Dermatol, 2001. **117**(5): p. 1282-9.
10. Cha, J. and V. Falanga, *Stem cells in cutaneous wound healing.* Clin Dermatol, 2007. **25**(1): p. 73-8.
11. Etufugh, C.N. and T.J. Phillips, *Venous ulcers.* Clin Dermatol, 2007. **25**(1): p. 121-30.
12. Schonfeld, W.H., et al., *An economic assessment of Apligraf (Graftskin) for the treatment of hard-to-heal venous leg ulcers.* Wound Repair Regen, 2000. **8**(4): p. 251-7.
13. McBeath, R., et al., *Cell shape, cytoskeletal tension, and RhoA regulate stem cell lineage commitment.* Dev. Cell, 2004. **6**: p. 483-495.
14. Fathke, C., et al., *Contribution of bone marrow-derived cells to skin: collagen deposition and wound repair.* Stem Cells, 2004. **22**(5): p. 812-22.
15. Hardy, S.A., D.J. Maltman, and S.A. Przyborski, *Mesenchymal stem cells as mediators of neural differentiation.* Curr. Stem Cell Res. Ther. , 2008. **3**: p. 43-52.
16. Porada, C.D., E.D. Zanjani, and G. Almeida-Porad, *Adult mesenchymal stem cells: a pluripotent population with multiple applications.* Curr. Stem Cell Res. Ther., 2006. **1**: p. 365-369.
17. Delorme, B., et al., *Specific plasma membrane protein phenotype of culture-amplified and native human bone marrow mesenchymal stem cells.* Blood, 2008. **111**(5): p. 2631-5.
18. Zappia, E., et al., *Mesenchymal stem cells ameliorate experimental autoimmune encephalomyelitis inducing T-cell anergy.* Blood, 2005. **106**(5): p. 1755-61.

19. Xu, G., et al., *Immunosuppressive properties of cloned bone marrow mesenchymal stem cells.* Cell Res, 2007. **17**(3): p. 240-8.
20. Wu Y, C.L., Scott PG, Tredget EE., *Mesenchymal stem cells enhance wound healing through differentiation and angiogenesis.* Stem Cells., 2007. **25**(10): p. 2648-59.
21. Yamaguchi, Y., et al., *Bone marrow cells differentiate into wound myofibroblasts and accelerate the healing of wounds with exposed bones when combined with an occlusive dressing.* Br J Dermatol, 2005. **152**(4): p. 616-22.
22. Chen, L., et al., *Paracrine factors of mesenchymal stem cells recruit macrophages and endothelial lineage cells and enhance wound healing.* PLoS ONE, 2008. **3**(4): p. e1886.
23. Horwitz, E.M., et al., *Isolated allogeneic bone marrow-derived mesenchymal cells engraft and stimulate growth in children with osteogenesis imperfecta: Implications for cell therapy of bone.* Proc Natl Acad Sci U S A, 2002. **99**(13): p. 8932-7.
24. Yamada, K.M. and B. Geiger, *Molecular interactions in cell adhesion complexes.* Curr Opin Cell Biol, 1997. **9**(1): p. 76-85.
25. Huveneers, S., H. Truong, and H.J. Danen, *Integrins: signaling, disease, and therapy.* Int J Radiat Biol, 2007. **83**(11-12): p. 743-51.
26. Maheshwari, G., et al., *Cell adhesion and motility depend on nanoscale RGD clustering.* J Cell Sci, 2000. **113 (Pt 10)**: p. 1677-86.
27. Cavalcanti-Adam, E.A., et al., *Cell spreading and focal adhesion dynamics are regulated by spacing of integrin ligands.* Biophys J, 2007. **92**(8): p. 2964-74.
28. Mao, Y. and J.E. Schwarzbauer, *Fibronectin fibrillogenesis, a cell-mediated matrix assembly process.* Matrix Biol., 2005. **24**: p. 389-399.
29. Pereira, M., et al., *Engineered cell-adhesive nanoparticles nucleate extracellular matrix assembly.* Tissue Eng, 2007. **13**(3): p. 567-78.
30. Sharma, R.I., et al., *Albumin-derived nanocarriers: substrates for enhanced cell adhesive ligand display and cell motility.* Biomaterials, 2006. **27**: p. 3589-3598
31. Salinas, C.N. and K.S. Anseth, *The influence of the RGD peptide motif and its contextual presentation in PEG gels on human mesenchymal stem cell viability.* J Tissue Eng Regen Med, 2008. **2**(5): p. 296-304.
32. Salinas, C.N. and K.S. Anseth, *The enhancement of chondrogenic differentiation of human mesenchymal stem cells by enzymatically regulated RGD functionalities.* Biomaterials, 2008. **29**(15): p. 2370-7.
33. Alvarez-Barreto, J.F., et al., *Preparation of a functionally flexible, three-dimensional, biomimetic poly(L-lactic acid) scaffold with improved cell adhesion.* Tissue Eng, 2007. **13**(6): p. 1205-17.
34. Wysocki, A.B. and F. Grinnell, *Fibronectin profiles in normal and chronic wound fluid.* Lab Invest, 1990. **63**(6): p. 825-31.
35. Labat-Robert, J., et al., *Plasma and tissue fibronectin in diabetes.* Clin Physiol Biochem, 1984. **2**(1): p. 39-48.
36. Herrick, S.E., et al., *Sequential changes in histologic pattern and extracellular matrix deposition during the healing of chronic venous ulcers.* Am J Pathol, 1992. **141**(5): p. 1085-95.
37. Steingen, C., et al., *Characterization of key mechanisms in transmigration and invasion of mesenchymal stem cells.* J Mol Cell Cardiol, 2008. **44**(6): p. 1072-84.

38. Ip, J.E., et al., *Mesenchymal stem cells use integrin beta1 not CXC chemokine receptor 4 for myocardial migration and engraftment.* Mol Biol Cell, 2007. **18**(8): p. 2873-82.
39. Sharma, R.I., et al., *Albumin-derived nanocarriers: substrates for enhanced cell adhesive ligand display and cell motility.* Biomaterials, 2006. **27**(19): p. 3589-98.
40. Doyle, A.D., et al., *One-dimensional topography underlies three-dimensional fibrillar cell migration.* J Cell Biol, 2009. **184**(4): p. 481-90.
41. McBeath, R., et al., *Cell shape, cytoskeletal tension, and RhoA regulate stem cell lineage commitment.* Dev Cell, 2004. **6**(4): p. 483-95.
42. Yim, E.K., S.W. Pang, and K.W. Leong, *Synthetic nanostructures inducing differentiation of human mesenchymal stem cells into neuronal lineage.* Exp Cell Res, 2007. **313**(9): p. 1820-9.
43. Goffin, J.M., et al., *Focal adhesion size controls tension-dependent recruitment of alpha-smooth muscle actin to stress fibers.* J Cell Biol, 2006. **172**(2): p. 259-68.
44. Schwartz, M.A. and M.H. Ginsberg, *Networks and crosstalk: integrin signalling spreads.* Nat Cell Biol, 2002. **4**(4): p. E65-8.
45. Lehnert, D., et al., *Cell behaviour on micropatterned substrata: limits of extracellular matrix geometry for spreading and adhesion.* J Cell Sci, 2004. **117**(Pt 1): p. 41-52.
46. Schmalenberg, K.E., H.M. Buettner, and K.E. Uhrich, *Microcontact printing of proteins on oxygen plasma-activated poly(methyl methacrylate).* Biomaterials, 2004. **25**(10): p. 1851-7.
47. Lee, K.B., et al., *Protein nanoarrays generated by dip-pen nanolithography.* Science, 2002. **295**(5560): p. 1702-5.
48. Lee, L.M., et al., *Low melting point agarose as a protection layer in photolithographic patterning of aligned binary proteins.* Lab Chip, 2006. **6**(8): p. 1080-5.
49. Tziampazis, E., J. Kohn, and P.V. Moghe, *PEG-variant biomaterials as selectively adhesive protein templates: model surfaces for controlled cell adhesion and migration.* Biomaterials, 2000. **21**(5): p. 511-20.
50. Langowski, B.A. and K.E. Uhrich, *Microscale plasma-initiated patterning (muPIP).* Langmuir, 2005. **21**(23): p. 10509-14.
51. Langowski, B.A. and K.E. Uhrich, *Oxygen plasma-treatment effects on Si transfer.* Langmuir, 2005. **21**(14): p. 6366-72.
52. Wu, Y., et al., *Mesenchymal stem cells enhance wound healing through differentiation and angiogenesis.* Stem Cells, 2007. **25**(10): p. 2648-59.
53. Discher, D.E., D.J. Mooney, and P.W. Zandstra, *Growth factors, matrices, and forces combine and control stem cells.* Science, 2009. **324**(5935): p. 1673-7.
54. Velnar, T., T. Bailey, and V. Smrkolj, *The wound healing process: an overview of the cellular and molecular mechanisms.* J Int Med Res, 2009. **37**(5): p. 1528-42.
55. Komarcevic, A., *[The modern approach to wound treatment]*. Med Pregl, 2000. **53**(7-8): p. 363-8.
56. Okumura, M., et al., *Effect of basic fibroblast growth factor on wound healing in healing-impaired animal models.* Arzneimittelforschung, 1996. **46**(5): p. 547-51.
57. Schneider, A., J.A. Garlick, and C. Egles, *Self-assembling peptide nanofiber scaffolds accelerate wound healing.* PLoS ONE, 2008. **3**(1): p. e1410.

58. Shen, Y.H., M.S. Shoichet, and M. Radisic, *Vascular endothelial growth factor immobilized in collagen scaffold promotes penetration and proliferation of endothelial cells.* Acta Biomater, 2008. **4**(3): p. 477-89.
59. Patel, S., et al., *Bioactive nanofibers: synergistic effects of nanotopography and chemical signaling on cell guidance.* Nano Lett, 2007. **7**(7): p. 2122-8.
60. Wang, R., et al., *Fibronectin's central cell-binding domain supports focal adhesion formation and Rho signal transduction.* J Biol Chem, 2005. **280**(31): p. 28803-10.
61. Langer, K., et al., *Optimization of the preparation process for human serum albumin (HSA) nanoparticles.* Int J Pharm, 2003. **257**(1-2): p. 169-80.
62. Hazra, A.K., S.P. Chock, and R.W. Albers, *Protein determination with trinitrobenzene sulfonate: a method relatively independent of amino acid composition.* Anal Biochem, 1984. **137**(2): p. 437-43.
63. Naczynski, D.J., et al., *Albumin nanoshell encapsulation of near infrared excitable rare earth nanoparticles enhances biocompatibility and enables targeted cell imaging.* Small, 2010.
64. Wang, G., et al., *Preparation of BMP-2 containing bovine serum albumin (BSA) nanoparticles stabilized by polymer coating.* Pharm Res, 2008. **25**(12): p. 2896-909.
65. Michaelis, K., et al., *Covalent linkage of apolipoprotein e to albumin nanoparticles strongly enhances drug transport into the brain.* J Pharmacol Exp Ther, 2006. **317**(3): p. 1246-53.
66. Mo, Y., et al., *Human serum albumin nanoparticles for efficient delivery of Cu, Zn superoxide dismutase gene.* Mol Vis, 2007. **13**: p. 746-57.
67. Spankuch, B., et al., *Downregulation of Plk1 expression by receptor-mediated uptake of antisense oligonucleotide-loaded nanoparticles.* Neoplasia, 2008. **10**(3): p. 223-34.
68. Ogawara, K., et al., *Pre-coating with serum albumin reduces receptor-mediated hepatic disposition of polystyrene nanosphere: implications for rational design of nanoparticles.* J Control Release, 2004. **100**(3): p. 451-5.
69. Kreuter, J., et al., *Covalent attachment of apolipoprotein A-I and apolipoprotein B-100 to albumin nanoparticles enables drug transport into the brain.* J Control Release, 2007. **118**(1): p. 54-8.
70. Rhaese, S., et al., *Human serum albumin-polyethylenimine nanoparticles for gene delivery.* J Control Release, 2003. **92**(1-2): p. 199-208.
71. Curran, J.M., Z. Tang, and J.A. Hunt, *PLGA doping of PCL affects the plastic potential of human mesenchymal stem cells, both in the presence and absence of biological stimuli.* J Biomed Mater Res A, 2008.
72. Sieg, D.J., et al., *FAK integrates growth-factor and integrin signals to promote cell migration.* Nat Cell Biol, 2000. **2**(5): p. 249-56.
73. Miyamoto, S., et al., *Integrins can collaborate with growth factors for phosphorylation of receptor tyrosine kinases and MAP kinase activation: roles of integrin aggregation and occupancy of receptors.* J Cell Biol, 1996. **135**(6 Pt 1): p. 1633-42.
74. Bourke, S.L. and J. Kohn, *Polymers derived from the amino acid L-tyrosine: polycarbonates, polyarylates and copolymers with poly(ethylene glycol).* Adv Drug Deliv Rev, 2003. **55**(4): p. 447-66.

75. Sung, H.J., et al., *Angiogenic competency of biodegradable hydrogels fabricated from polyethylene glycol-crosslinked tyrosine-derived polycarbonates.* Eur Cell Mater, 2008. **15**: p. 77-87.
76. Tangpasuthadol, V., S.M. Pendharkar, and J. Kohn, *Hydrolytic degradation of tyrosine-derived polycarbonates, a class of new biomaterials. Part I: study of model compounds.* Biomaterials, 2000. **21**(23): p. 2371-8.
77. Tangpasuthadol, V., et al., *Hydrolytic degradation of tyrosine-derived polycarbonates, a class of new biomaterials. Part II: 3-yr study of polymeric devices.* Biomaterials, 2000. **21**(23): p. 2379-87.
78. Yu, C. and J. Kohn, *Tyrosine-PEG-derived poly(ether carbonate)s as new biomaterials. Part I: synthesis and evaluation.* Biomaterials, 1999. **20**(3): p. 253-64.
79. Yu, C., et al., *Tyrosine-PEG-derived poly(ether carbonate)s as new biomaterials. Part II: study of inverse temperature transitions.* Biomaterials, 1999. **20**(3): p. 265-72.

CURRICULUM VITAE

Jing Xu

Education:

M.S. in Cell and Developmental Biology (May 2010)
Rutgers University, Piscataway, New Jersey

M.S. in Pathology, 2006
Tsinghua University & Peking Union Medical College, Beijing, China

M.D., 2003
Southeast University, Nanjing, China

Research Positions:

08/2009-05/2010 IGERT Fellow
IGERT (Integrative Graduate Education and Research Traineeship), Rutgers-NSF

08/2007-07/2009 Graduate Assistant,
Rutgers University, Dept. of Biomedical Engineering

08/2006-07/2007 Graduate Research Fellow,
Rutgers-UMDNJ, Program of Molecular Biosciences

09/2003-06/2006 Research Assistant,
Tsinghua University & Peking Union Medical College, Beijing, China